PALEOCEANOGRAPHY, VOL. 12, NO. 2, PAGES 281-305, APRIL 1997

# Simulated ocean circulation and sediment transport in the North Atlantic during the last glacial maximum and today

Dan Seidov

Geologisch–Paläontologisches Institut, Universität Kiel, Kiel, Germany

Bernd J. Haupt

Sonderforschungsbereich 313, Universität Kiel, Kiel, Germany

**Abstract.** Paleocirculation of the North Atlantic Ocean at the last glacial maximum (LGM) is simulated using a large–scale ocean general circulation model (OGCM). The model is driven by glacial sea surface thermohaline conditions and wind stress. For comparison of past and present circulation patterns, a separate run provides the Holocene/modern circulation patterns based on the present day sea surface climatology. The output of the OGCM is then used in a sedimentation model and in a model to trace water parcel trajectories. The sedimentation model reveals the differences in sediment deposition in the North Atlantic linked to past and present circulation regimes. The trajectory–tracing model facilitates a better understanding of the thermocline and deep ocean ventilation, the actual three–dimensional conveying of water, and the role of convection in maintaining the meridional thermohaline overturning. The results of the trajectory–tracing technique indicate stronger subtropical thermocline ventilation during the LGM. For the deep ocean currents, we find severe alteration of three–dimensional water motion in response to weakening of the LGM convection and its retreat to the southwest from its present locations. Ocean circulation models can provide sedimentation studies with information on the circulation regime that proxy data used alone cannot. These is because such models furnish both circulation patterns and the ventilating convection depths.

## Introduction

The modern paradigm of world ocean thermohaline circulation is that the system is driven by the production of North Atlantic Deep Water (NADW) at several tiny sites in the northern North Atlantic and the Norwegian–Greenland Seas (NGS) initiating the global thermohaline conveyor [*Gordon*, 1986; *Broecker*, 1991; *Schmitz*, 1995]; (see also the review by *Gordon et al.*, [1992]). Isopycnal surfaces outcrop in the ventilation regions causing water to descend along the isopycnals into the deep ocean. This descending water forms a southward deep ocean outflow from the NADW formation areas. A compensating northward flow develops in the upper layers to replace the newly formed deepwater outflow. We refer to this major cell of the North Atlantic meridional circulation as a "forward conveyor." In the absence of an opposing abyssal current, NADW would fill the entire deep ocean. Such complete dominance of the NADW is, however, prevented by the northward incursion of the Antarctic Bottom Water (AABW). This secondary yet very important gyre comprising the AABW northward incursion is referred to as a "deep ocean reverse conveyor." At the surface the Ekman drift currents form the divergence in the middle to high latitudes and convergence in the subtropics. This leads to an "upper ocean reverse conveyor," a shallow upper ocean gyre with wind–induced equatorward transport in the uppermost layers. The interplay and delicate balance of these three gyres determines the modern ocean climate as reflected in observed thermohaline patterns [*Levitus*, 1982; *Levitus and Boyer*, 1994; *Levitus et al.*, 1994]. Today, the strong forward conveyor is a dominant feature of meridional overturning pattern.

Proxy data analysis indicates that the glacial North Atlantic conveyor operated differently from the present one, causing different modes of circulation [*Boyle and Keigwin*, 1987; *Broecker and Denton*, 1989; *Broecker*, 1991; *Keigwin et al.*, 1991; *Bond et al.*, 1992; *Lehman and Keigwin*, 1992; *Sarnthein et al.*, 1994, 1995; *Maslin et al.*, 1995; *Oppo et al.*, 1995]; (see also the review by *Bond* [1995]). After pioneer work by *Bryan* [1986], many recent numerical simulations of widely different complexity confirmed that multiple stable modes of a buoyancy–driven conveyor may indeed occur [*Manabe and Stouffer*, 1988, 1995; *Marotzke and Willebrand*, 1991; *Weaver and Sarachik*, 1991; *Wright and Stocker*, 1991; *Fichefet and Hovine*, 1993; *Fichefet et al.*, 1994; *Maier–Reimer et al.*, 1993; *Weaver et al.*, 1993; *Rahmstorf*, 1994, 1995; *Stocker*, 1994; *Weaver and Hughes*, 1994; *Sakai and Peltier*, 1995].

We use ocean surface data to simulate the past and present North Atlantic circulation pattern by means of an ocean general circulation model (OGCM). The model is driven by wind



Paper number 96PA03444
0883–8305/97/96PA–03444$12.00

stress, and by the heat and freshwater fluxes calculated from specified sea surface temperature (SST) and sea surface salinity (SSS). The OGCM runs yield three–dimensional (3–D) temperature, salinity, and velocity fields relevant to the Holocene/modern (HM) and the sea surface conditions at the last glacial maximum (LGM) at 18.000 ka. The LGM time slice has the largest data set of SSS and SST available of any glacial period and has been updated recently in the northern North Atlantic [*Sarnthein et al.*, 1995]. These data define the surface boundary conditions needed to address a critical question concerning operation of the salinity conveyor belt in the high–latitude North Atlantic at the LGM.

We formulate our task as a modeling attempt that recruits a major simulation technique, the OGCM, and two complementary models that quantify the sediment transport and the three–dimensional water motion with ventilation in high latitudes. We show that such a threefold modeling approach will enhance past ocean circulation studies employing ocean general circulation models. These two additional components, a sediment transport model and a trajectory–tracing model, help to reduce ambiguities in proxy data and simulation analysis. We demonstrate how these additional computations help constrain the interpretation of circulation patterns which emerge in simulations of ancient oceans. In particular, we show how these calculations can be used to understand ventilation of the ocean and to validate the circulation changes by interpretation of the sedimentation patterns linked to those changes. This type of constraint may be especially useful for simulating ocean currents for time periods with poorly documented hydrophysical conditions. Using this threefold approach, even a limited knowledge of historical sediment patterns in some key areas would be instrumental in reducing the ambiguity due to lack of ocean paleoclimatic data for those times.

The flow velocity vectors from OGCMs are computed on a numerical grid at fixed points in space. This traditional Eulerian representation of a flow has some disadvantages when the actual 3–D water transport is of particular interest. Firstly, horizontal velocity maps fail to show the horizontal and vertical motion of the water masses simultaneously. Secondly, even if a 3–D velocity pattern is plotted, or if horizontal vectors' maps are analyzed in parallel with scalar maps of the vertical velocity components, one would nonetheless miss the important part of convection due to hydrostatic instability. Ventilation of the deep ocean would be missed in a traditional Eulerian visualization of ocean circulation. We apply a model that traces the trajectories of Lagrangian particles (i.e., neutrally buoyant particles therefore moving together with the water parcels) in order to visualize 3–D water transport. To our knowledge this approach has not been used in paleoceanographic studies except for the first attempt by *Haupt et al.* [1994]. Here the method is updated to include the impact of convection, and it is applied to the interpretation of changes in the thermocline and deep ocean ventilation at the LGM.

Another problem inherently linked to modeling of past ocean circulation is the simulation of sedimentation and sediment transport. Typically, sedimentation is employed to reconstruct ocean currents that have enabled an observed sediment drift. Provided that the glacial circulation patterns differed from the modern velocity distribution, the glacial sedimentation and particle transport also inevitably had to be different. Many attempts have been made to infer the circulation pattern from sediment structure and especially from ice–rafted debris [*Goldschmidt et al.*, 1992; *Honjo*, 1990; *Pfirmann et al.*, 1990; *Seibold and Berger*, 1993, *Goldschmidt*, 1995].

Theoretically, if one knew the historical circulation patterns for certain consecutive time periods, then there would be no fundamental difficulty in solving the inverse problem: reconstruction of historical distributions of the sediment throughout the basin. In practice, however, this task is not as straightforward as one might expect. Yet recently, some authors have addressed the issue showing that the approach may be useful [*Sündermann*, 1983; *Sündermann and Klöcker*, 1983; *Tetzlaff and Harbaugh*, 1989; *Bitzer and Pflug*, 1990; *Syvitski and Hughes*, 1992].

We try to solve a reverse problem by applying a 3–D sedimentation model to complement the circulation study using the OGCM and calculate sedimentation patterns that would correspond to the simulated glacial North Atlantic Ocean circulation. On the basis of the sediment patterns calculated using the HM and the LGM velocity fields, one may arrive at more definite conclusions about the near–bottom currents than would arise from studying the velocity patterns alone. The new feature here is a simulation of the eolian sediment rates relevant to the circulation in the entire glacial North Atlantic. These calculations show the changes in the routes of the near–bottom currents and provide sedimentation rates and sediment distribution patterns that can be compared to observations. Previously, the 3–D sediment transport model has been applied to the northern North Atlantic Ocean only [*Haupt et al.*, 1994], and therefore could not shed light on one of the most discussed paleoceanographic problems concerning the glacial conveyor dynamics.

In summary, our task is to evaluate the circulation pattern, the sediment transport, and the actual 3–D water motion on the basis of the HM and LGM sea surface conditions. The goal is to compute, visualize, and comprehend glacial–to–interglacial changes in the ocean circulation of the North Atlantic by means of three numerical models: (1) a large–scale ocean general circulation model; (2) a sedimentation and sediment transport model, and (3) a model for tracing neutrally buoyant particles. The sediment transport model facilitates a better understanding of the deep ocean circulation. The trajectory–tracing model computes the actual 3–D trajectories of water volumes and is instrumental in comprehending ventilation of the thermocline and the deep ocean.

In a sense, the sedimentation model and the trajectory–tracing model are the 'add–ons' to the OGCM. First the circulation has been simulated using an OGCM on the basis of sea surface conditions relevant to the LGM and, for comparison, to the HM time slice. Next, the sediment transport model has been initialized and driven by the OGCM output (temperature, salinity, velocity, and convection depths) to calculate the sedimentation rates linked to the two corresponding circulation patterns. Subsequently, the velocities and convection depths calculated in the OGCM have been applied in the trajectory–tracing model to track down the 3–D transport pathways of water parcels at these two time slices.

## Numerical Models

**Ocean circulation model.** We employ a planetary geostrophic ocean circulation model especially designed for coarse–resolution, large–scale ocean circulation studies described by *Seidov* [1996] and *Seidov and Prien* [1996]. This model belongs to the "intermediate" or "planetary geostrophic" class of models [*Hasselmann*, 1982; *Seidov*, 1986, 1996; *Colin de Verdière* , 1988; *Maier–Reimer et al.*, 1991, 1993; *Zhang et al.*, 1992]. Except for the linear dynamics inherent to planetary geostrophic models, such models retain all features of the most advanced primitive equation models (PEM) that are the present–day standards in physical oceanography [e.g., *Bryan*, 1969, *Cox*, 1984, *Semtner*, 1986]. The planetary geostrophic models are based on the idea that the momentum balance away from the equator is predominantly geostrophic. Different closure hypotheses are used to satisfy side boundary conditions, with Laplacian friction the most often employed. When lateral friction is included or parameterized, planetary geostrophic models converge to a primitive equation formulation with linear dynamics [*Colin de Verdière*, 1988; *Maier–Reimer et al.*, 1993]. Planetary geostrophic formalism allows some simplifications of the momentum and vorticity balance equations, and a longer time step, and consequently becomes computationally more effective. Parallel runs have been made on a coarse–resolution grid using this model and the Geophysical Fluid Dynamics Laboratory (GFDL) modular ocean model [*Bryan*, 1969; *Cox*, 1984; *Pacanowski et al.*, 1993], a PEM. *Seidov and Prien* [1996] have shown that results of this planetary geostrophic model match well with the performance of the GFDL model.

Any OGCM contains a procedure to allow convective mixing that develops due to hydrostatic instability if denser water is formed (or advected) over lighter water. This is the key process for deep water production and transport. As done commonly in an OGCM, this instability is accommodated by mixing water vertically until it regains complete hydrostatic stability [*Cox*, 1984]. This vertical adjustment takes place as a step process with several successive mixings of adjacent layers until complete hydrostatic stability is restored. As the water convects, the particles associated with the mixing volumes exchange their positions vertically, and hence the convection facilitates deep ventilation. We argue below that it is the convection that makes the results of a numerical circulation model a unique source of data for any study requiring the velocity field. For instance, convection is central to a study of deep ocean ventilation inferred from ocean hydrography. Indeed, hydrostatic instability is usually removed from climatological data sets [e.g., *Levitus*, 1982; *Levitus and Boyer*, 1994; *Levitus et al.*, 1994]. When available, direct velocity measurements are not commonly supplemented by information on the occurrence of deep convection in situ and on the depth of its penetration. It is clear, however, that particles drifting (and settling, if not neutrally buoyant, as sediment) in a water parcel would be carried abruptly to different depths if convection does occur.

**Ocean sedimentation model.** The sedimentation model employed here was designed by *Haupt* [1995] and tested in *Haupt et al.* [1994, 1995]. It is a large–scale sedimentation model consisting of two components: (1) a 3–D sediment transport model in the ocean interior, and (2) a 2–D sediment transport model in a thin near–bottom layer following smoothed bottom topography. The 3–D component models the advection–diffusion of sediment similar to the equations of advection–diffusion of heat and salt in the OGCM, and includes an added term to compute the settling of sediment in the water column.

Since the box method of *Bryan* [1969] is used to construct the 3–D numerical grid in the OGCM employed, the bottom topography in the OGCM is of a staircase type (Figure 1). A technique for smoothing this staircase bathymetry for use in the 2–D sediment transport submodel is discussed by *Haupt et al.* [1994]. In our experiments (see below), the bottom slope replacing the staircase–type topography never exceeds 5°, and therefore the near–bottom flow never detaches from the seabed. Hence the staircase–type approximation of bottom topography is legitimate for our both OGCM and 3–D sediment transport computations [*Puls*, 1981]. The 3–D and 2–D submodels are coupled by vertical exchange of suspended sediment. This exchange is important for redistribution of sediments. If erosion takes place, or if there is already some suspended sediment in the 2–D bottom layer, sediment can reenter the three–dimensional ocean circulation. This technique enables redistribution of sediment by reduced bottom currents [*Sündermann*, 1983] depending on the amount of sediment available in the bottom layer.

The sediment transport model has been proven capable of simulating sediment dynamics incorporating the processes of resuspension and redeposition of both terrigenous and biogenic sediments. The 3–D component of the sedimentation model simulates the lateral transport and the entry of sediment particles at the sea surface, including the enter of ice–rafted sedimentary material. The mass of sediment covering the seafloor depends only on the balance of sources and sinks, whereas the spatial variation of the sediment rates depends on the circulation pattern and the particle grain size. The 2–D model is initialized at every time step by the exchange of sediment between the ocean body and the ocean floor. The sediment in the bottom layer is transported by a corrected benthic flow which is largely a projection of the OGCM velocity field onto the smoothed bottom layer (1 cm thick). Additionally, the near–bottom velocities are reduced to take bottom friction into account [*Miller et al.*, 1977; *Zanke*, 1978; *Sündermann*, 1983].

We have noted above that the equation for 3–D sediment concentration is principally similar (except for the settling term) to the OGCM equations for 3–D advection–diffusion of heat and salt. We solve this equation numerically in exactly the same manner as we do it in the OGCM. If this concentration equation were to be solved as a passive tracer equation in the OGCM, the convection due to hydrostatic instability would be applied to this concentration as to any other tracer [*Cox*, 1984; *Pacanowski et al.*, 1993]. When the velocity fields are used in the concentration equation of the sediment transport model, the information about convection must be included to make concentration evolution compatible with that for other tracers in the OGCM. The impact of convection was not included in the previous version of the sedimentation

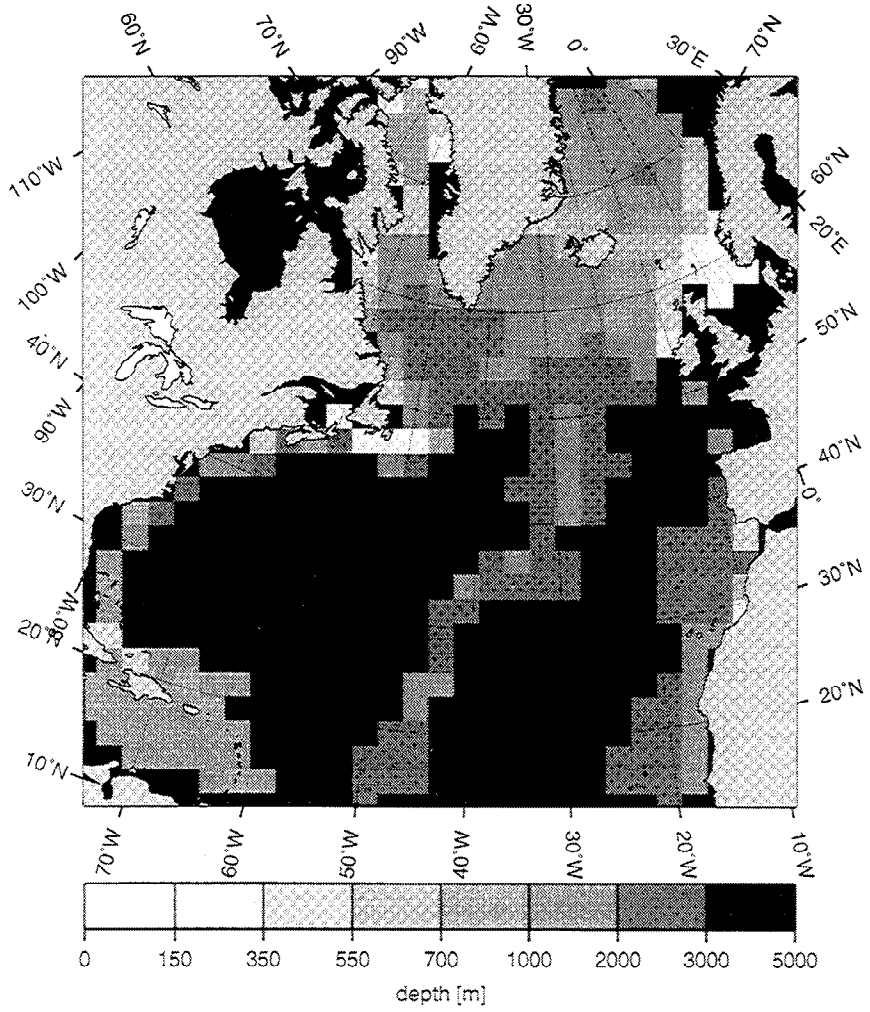


**Figure 1.** Model bottom topography of the North Atlantic on a 2°x2° grid. Iceland and the Caribbean are presented as seamounts to enable coarse resolution in a single–connected domain.

model [*Haupt et al.*, 1994]. Here vertical mixing, similar to that employed in the OGCM, is applied to concentration when necessary. The sediment transport model 'knows' when to mix water because we have encoded the convection depths in the velocity field as an additional parameter. When used in the sedimentation model, this information is decoded to enable vertical mixing in the grid points where convection occurs (see below in the discussion of the convection patterns).

**Particle–tracing model**. The water volume trajectory–tracing model was developed by *Haupt* [1995] and was employed to trace particle drifts in the northern North Atlantic [*Haupt et al.*, 1994, 1995]. This model exercises a hybrid Eulerian–Lagrangian (or semi–Lagrangian) approach; the velocity components are interpolated to the current positions of the Lagrangian particles from the nearby grid points of an Eulerian numerical grid. As in the sediment transport model described above, the Eulerian velocity field is provided by the OGCM, whereas the coordinates of Lagrangian particles are calculated straightforwardly, using the Lagrangian velocity along the trajectory. More details about the design and use of both models are given by *Haupt* [1995] and *Haupt et al.* [1994, 1995].

Convection is recognized to be an important component of thermohaline circulation in spite of the small percentage of the world ocean it affects directly [*Killworth*, 1983]. Physically, convection does not transport water in the same manner as advection. It mixes water vertically in water columns or "chimneys" [*Send and Marshall*, 1995]. As we have emphasized above, ventilating convection induced by hydrostatic instability is included in all three components of our simulations. The semi–Lagrangian trajectory–tracing model calls, however, for a different convective procedure to exercise vertical ventilation. Here the velocity field is supplemented by the convection depths showing where and to what depth the vertically mixing volume should be propelled in the turbulent chimney. The convection depths indicate how many pairs of layers participate in mixing, i.e. to which layer the particle entering the chimney must be transported. The rule is that particles entering the convective chimney at the top are propelled downward to the base of the chimney and, conversely,

particles are propelled upward to the uppermost layer if they enter the chimney at its base. The mixing volumes change position vertically as many times as prescribed by convection depths (showing how many layers are affected by convection). However, for every mixing parcel, the mixing occurs only once, that is, when the parcel enters the convection site. This mechanism is consistent with the convection scheme employed in the OGCM. Moreover, such an interpretation of the convective mixing follows the concept of the so–called transilient turbulence [*Stull,* 1984] introduced in order to simulate distant turbulent mixing produced by large eddies.

## Experimental Design and Surface Boundary Conditions for the Ocean Circulation Modeling

**Circulation model.** As we want to model the ocean circulation based on proxy data rather than perform another sensitivity study, only the domain comprising a basin from 10°N to 80°N is adopted for simulations. These latitudinal limits are used because reliable SSS, arranged on a regular grid covering an extended area and suitable for numerical modeling, is currently available only in the region north of 40°N. However, the North Atlantic branch of the conveyor cannot be modeled without at least including the subtropical region. The salinity conveyor belt is driven by convection and newly formed deep water outflow at high latitude, but convection itself occurs due to the cooling of warm salty water brought by the conveyor from the subtropics.

In order to study the present–day conveyor dynamics, it is more advisable to employ a whole Atlantic model, or better a global ocean model, rather than the regional North Atlantic model as we do here. In fact, all large–scale sensitivity studies of the conveyor are run globally. On the other hand, if one extends the domain too far to the south, a study of any past ocean circulation would meet great uncertainties because of problems with paleo–SSS in the Southern Ocean (that is, we cannot currently assemble reliable SSS conditions over a regular grid in the southern hemisphere). Instead, we have extended the domain to 10°N and introduced a sponge layer at the southern boundary to restore the numerical solution to modern climatology in a narrow latitudinal belt near this latitude. This is equivalent to assuming that the impact of the Antarctic Intermediate Water (AIW) and AABW was the same at the LGM as it is today.

We do not advocate regional modeling in principle. For example, the distribution of tracers, such as $\delta^{13}C$, and ages of water cannot be modeled regionally. Circulation patterns, however, can be inferred in a regional model with a large degree of certainty. This has been proven by many authors, including those who have addressed mesoscale dynamics of the North Atlantic [*Sarmiento,* 1986; *Bryan and Holland,* 1989; *Böning et al.,* 1991]. We note, however, that in the those studies the sponge layer was placed at 30°S. Nevertheless, the trade winds and equatorial upwelling provide a well–defined physical boundary at 10°–15°N. The planetary geostrophic model converges to a primitive equation model everywhere except near the equator. Hence we believe that 10°N is probably the best compromise to overcome the lack of proxy data and still produce meaningful results. Since we try to justify our results using the existing evidence, we put forth these reservations due to principal shortcomings in regional modeling. In the end, only comparison to observations can justify or refute the approach. D. Seidov and A. Paul [Modelling the glacial and meltwater Atlantic circulation, submitted to *Paleoceanography,* 1996] have compared paleocirculation patterns in the North Atlantic using one global and two regional North Atlantic models. It has been found that the regionally modeled conveyor dynamics, though somewhat deteriorated because of a sponge layer surrogate of the real water exchange, still represent the major glacial–to–interglacial changes quite reasonably. This comparison is not entirely reliable because SSS data in the southern hemisphere are incomplete and very sparse. Nevertheless, we can at least argue that one would not arrive at decisively better results concerning the overturning and 3–D circulation pattern in the North Atlantic if global circulation were used with the existing data.

Numerical solutions to the OGCM equations are obtained on a regular numerical grid with 2°x2° horizontal resolution and 12 vertical levels unevenly spaced from the surface to the bottom depth at 4.6 km. The middle depths of the layers occur at 50, 150, 250, 350, 450, 550, 697, 965, 1400, 2050, 2943, and 4020 m, a resolution that seems to be sufficient for the case studies under consideration. The horizontal resolution is twice as coarse as that of *Seidov et al.* [1996]. Nonetheless, the quality of the thermohaline circulation computed on the 2°x2° grid does not differ greatly from that obtained on the 1°x1° grid [*Seidov and Prien,* 1996]. Many more experiments can be performed because of the coarser horizontal resolution, resulting in better model tuning. We note also that many details of geometry can be adequately resolved only in a fine–resolution, or eddy–resolving, numerical model. For instance, although the Denmark Strait is resolved by a 1°x1° grid, there are very few velocity grid points there. Moreover, variances of the glacial geometry and ice–covered glacial conditions in the channel are not precisely known.

Coarse resolution inevitably calls for a substantial simplification of the basin geometry and its morphology (Figure 1). As we employ the sedimentation model on a coarse grid, some additional consideration was necessary to assemble model bottom topography. For instance, the sediment transport may become largely distorted in the key area of the Denmark Strait on a 2°x2° grid and the suspended particles may become trapped in the Greenland–Iceland–Norwegian Seas as a result of the poor resolution. Therefore Iceland is treated as an undersea mountain. If one also treats the Caribbean islands as seamounts, a single–connected North Atlantic basin may be used, which noticeably speeds up calculation of the barotropic mode of the currents.

The ocean circulation model is driven by the momentum, heat, and freshwater fluxes specified or calculated at the sea surface. Wind stress supplies the momentum, whereas sea surface water characteristics (in the uppermost layer) are restored to the specified SST and SSS values. In the HM reference run (Table 1), the surface climatology was extracted from *Levitus* [1982]. The sea surface conditions for the LGM were assembled from different sources cited in Table 1. SST from Climate: Long Range Investigation Mapping and Prediction (CLIMAP) Project Members [1981] (hereafter re-

**Table 1.** Surface Data Sources for Numerical Experiments

| DATA | Time | |
|---|---|---|
| | HM | LGM |
| Wind stress | T42 wind stress | T42 wind stress calculated using *CLIMAP* [1981] surface conditions |
| Sea surface temperature (SST) | *Levitus* [1982] | *CLIMAP* [1981] LGM data, and data of *Schulz* [1994], and data of *Sarnthein et al.* [1992;1995] in the northern North Atlantic and NGS |
| Sea surface salinity (SSS) | *Levitus* [1982] | *Levitus* [1982] data south of 40°N increased by 0.8 psu and the recalculated SSS using $\delta^{18}O$ from *Duplessy et al.* [1991] north of 40°N, and *Sarnthein et al.* [1995] north of 50°N in the northern North Atlantic and NGS for LGM |

HM is Holocene/modern; LGM is last glacial maximum (18,000–15,000 $^{14}C$ years B.P.); NGS is Norwegian–Greenland Seas. T42 wind stress is an output from an atmospheric general circulation model provided by the Max Planck Institute for Meteorology, Hamburg and Bremen University [*Lorenz et al.*, 1996] (see text).

ferred to as *CLIMAP* [1981]) reconstructions was merged to the north of 50°N and east of 40°W with the most recent data from *Schulz* [1994].

It has been shown by many authors [e.g., *Bryan*, 1986; *Manabe and Stouffer*, 1988, 1995; *Maier–Reimer et al.*, 1991; *Marotzke and Willebrand*, 1991; *Fichefet et al.*, 1994; *Rahmstorf*, 1994, 1995; *Sakai and Peltier*, 1995; *Mikolajewicz*, 1996] that conveyor dynamics are most sensitive to high–latitude freshwater discharge. Although thermal and wind impact over the sea surface are both immensely important, even more concern should be given to the SSS compilation from different sources.

*Seidov et al.* [1996] modified modern SSS values for the LGM time period as following: North of about 40°N, SSS was combined from the *Levitus* [1982] data and the reconstructions of *Duplessy et al.* [1991] for the central part of the basin. In the region north of 40°N and west of 30°W, and also to the south of 40°N, the *Levitus* [1982] SSS data were first increased by 0.8 psu to fit them to the values given by *Duplessy et al.* [1991]. The data were merged and smoothed using a low–pass filter suggested by *Shapiro* [1971]. In high latitudes, salinity was calculated from SST and the planktonic $\delta^{18}O$ reconstructions by *Schulz* [1994], *Weinelt* [1993], and *Sarnthein et al.* [1995]. The *CLIMAP* [1981] SST was used everywhere except for the northeastern North Atlantic and the Nordic Seas, where it was updated from *Schulz* [1994] and *Sarnthein et al.* [1995].

Wind stress for the LGM is the newest release from the ECHAM–3/T42 atmospheric model, generated for paleoclimatic studies by the groups at Max Planck Institute in Hamburg and at Bremen University (*Lorenz et al.* [1996]; the setup of the T42 runs is of the type discussed by *Lautenschlager and Herterich* [1990] using the CLIMAP SST as surface condition). *Seidov et al.* [1996] interpolated July and January wind stresses from the T42 model onto a 1°x1° degree grid and smoothed them with a low–pass filter to suppress high–frequency noise (see above). For our study we have transferred these wind stress to the 2°x2° grid.

All surface data are specified as annual means of the July and January values. This definition of annual values helps to retain the same level of generality for both the HM and LGM runs. The LGM SST fields are reconstructed for the summer and winter seasons [*CLIMAP*, 1981; *Schulz*, 1994], whereas SSS is only available for the summer. Using only summer surface conditions for both SST and SSS would have jeopardized the calculations. Indeed, the conveyor dynamics could have been seriously deteriorated because of lighter NADW due to an abnormally warm sea surface in the high latitudes. Hence a compromise was adopted to treat the summer paleo–SSS to the north of 40°N as annual, whereas SST, wind stress, and SSS to the south of 40°N are annual mean fields.

Temperature and salinity of the uppermost layer (at 50 m) are restored to the specified SST and SSS with a relaxation time of 50 days [*Bryan*, 1987]. At the southern boundary a relaxation time of 1 year was chosen for restoring temperature and salinity to their modern values. This restoration period increases rapidly inward with no further restoration applied north of 16°N. Since the time relaxation toward ocean climatological data inside the sponge layer is much longer than the time relaxation at the sea surface, the SST and SSS anomalies affect not only the sea surface near the southern boundary but the deeper layers there as well. Therefore near the southern wall there is a mixture of the modern and the glacial hydrology which tends toward modern values only in the deepest layers.

Many control runs were performed using modern surface climatology to find the parameter set giving the best fit, in a coarse–resolution simulation, with present–day circulation of the North Atlantic. The task was to keep the thermocline structure, meridional overturning, and northward heat transport all in reasonable qualitative agreement with observations. Several sensitivity runs of increasing complexity were carried out to determine the relative importance of different factors owing to the new combination of the circulation, trajectory–tracing, and sediment transport models. Additional sensitivity runs were performed using the GFDL OGCM to ascertain that similarity of the model solutions would apply equally to all three components of our modeling effort. These parallel runs gave us the confidence that our study is at least free from a "model–dependent" bias.

The two major HM and LGM experiments, on the 2°x2° grid with 12 levels, real geometry, and bottom topography, were both extended well over 1000 years. Simulations in a domain the size of the North Atlantic under the restoring boundary condition do not call for such a long integration time to obtain a steady state (almost complete steady state was reached after approximately 300 years). However, the computations were continued over at least two or three turnover times passed to ensure complete formation of all water masses in the domain (turnover time for the North Atlantic only is estimated at 300–400 years). The results of the HM run serve two purposes: as the basis for comparison with the LGM run, and as a means of validating the model. Table 2 contains some aggregated parameters indicating that the model per-

**Table 2.** Ocean Circulation Parameters in the HM and LGM Numerical Experiments

| Parameters | Time | |
|---|---|---|
| | HM | LGM |
| [T], °C | 16.9 (17.8) | 13.0 |
| [S], psu | 35.50 (35.07) | 35.97 |
| {T}, °C | 7.0 (5.9) | 5.7 |
| {S}, psu | 35.12 (35.08) | 35.42 |
| {KE}, erg $cm^{-3}$ | 1.84 | 1.36 |
| {NHFL}, PW | 0.29 | 0.13 |
| $\{NHFL\}_{max}$, PW | 0.53 | 0.49 |
| {NADW}, Sv | 13.3 | 8.2 |

HM is Holocene/modern; LGM is last glacial maximum, [T] and [S] are temperature (degreees Celsius) and salinity (practical salinity units) of the uppermost layer (at 50 m) averaged over the sea surface; {T} and {S} are temperature and salinity averaged over the entire basin; {NHFL} is the northward heat flux (1 PW=$10^{15}$ Watt) averaged over the latitude; $\{NHFL\}_{max}$ is the maximal value of {NHFL}. {KE} is kinetic energy averaged over the entire basin, {NADW} is the value of North Atlantic Deep Water (NADW) production (see Figure 2; 1 Sv=$10^6$ $m^3s^{-1}$). Modern values of modern [T], [S], {T}, and {S} based on *Levitus* [1982] data set for the chosen geometry are shown in parentheses.

formed reasonably in the HM case and that the system behaved as generally expected under glacial conditions. The performance indicators, e.g., kinetic energy, meridional overturning, northward heat flux and its maximum positions, and temperature and salinity averaged over the surface and over the entire ocean volume, all fall in reasonable ranges common to most coarse–resolution and some low–order models of modern and glacial ocean circulation [e.g., *Bryan,* 1987; *Fichefet et al.,* 1994; *Maier–Reimer et al.*, 1993; *Rahmstorf,* 1994, 1995; *Weaver and Hughes*, 1994].

Note that the maps showing the results of the OGCM runs look similar to that presented by *Seidov et al.* [1996], although they are different in minor details. In principle, we could have just mentioned the maps presented in the cited work in view of this similarities. Yet since there are still some differences, and to maintain readable structure of the discussion of the sediment transport and particle tracing computations, we present some of the OGCM results to provide such a background.

**Sediment transport model.** All experiments with the sediment transport model are initialized with the same sediment properties (sediment sources, sinking velocity of 0.05 cm $s^{-1}$ = 43.2 m $d^{-1}$ [*Shanks* and *Trent,* 1980], density of sediment, grain size, and sedimentological grain diameter, form factor of sediment particles, and sediment porosity). The simulations were run over 1000 years. It is not possible to run the model to a steady state condition because of the forward integration (e.g., the bottom slope changes in time affect the critical velocities, critical erosion and suspension velocity, and, consequently the sediment transport itself). To take into account the eolian sediment input from the atmosphere, a relatively small flux of about $1.0x10^{-13}$ g $cm^{-2}s^{-1}$ (= 0.0864 mg $m^{-2}d^{-1}$) is prescribed at the uppermost layer following *Haupt et al.* [1994]. After settling, the eolian sediment is also available at the seafloor (the sediment particles can reenter the sediment flow because of turbulence). The settling velocities are higher than vertical water velocity by at least a factor of 10 everywhere except for the bottom slope, where they can be of the same magnitude. This implies that in the open ocean the sediment drifts reflect mainly the near–bottom (contour) currents. Hence they cannot help to visualize 3–D water transport or to interpret ventilation of the deep ocean; the trajectory–tracing model is our primary tool for this purpose.

**Trajectory–tracing model.** The trajectory–tracing model has been run over 500 years of model time using the steady state velocity field provided by the OGCM. The water parcels have no inherent sinking velocity (that is, they are neutrally buoyant), and therefore they move together with the water flow. The neutrally buoyant parcels have long been recognized as an ideal tool for tracking specific water volumes [e.g., *Cox and Bryan,* 1984; *Böning and Cox*, 1988]. For instance, they have been successfully used to address some aspects of thermocline ventilation [*Cox and Bryan,* 1984]. To validate the accuracy of the Lagrangian calculations, 2–D trajectories were calculated using a barotropic (essentially two–dimensional) velocity field. In this additional validating experiment, most trajectories stayed on closed streamlines, coinciding with isolines of the total stream function for a very long time (over 1000 years). Only in the central part of the subtropical gyre did some trajectories show a tendency to diverge from a closed streamline and to crowd in the center of the gyre after about 500–600 years of running along the streamlines. This happens because rounding errors limit the accuracy with which the vertically averaged velocity can satisfy the continuity equation. This flaw cannot be cured by a shorter time step. However, this deviation from completely nondivergent behavior of the barotropic flow is much smaller than true divergence of the baroclinic currents in this area and may therefore be neglected in 3–D runs. In another test run, more dense clouds of 100 particles have been launched in several areas to observe how the clouds' density can influence interpretations. We find that about 20 to 30 particles easily facilitate tracing of water parcels from areas of about 1000x1000 $km^2$ (deep water formation usually occupies areas of this size or smaller).

## Results of Numerical Experiments

**Thermohaline conveyor, convection and circulation patterns from OGCM.** To highlight the changes in volume transport and the buoyancy–induced alteration of circulation, a meridional "overturning" stream function is usually computed. This stream function delineates total transport from coast to coast in a vertical profile. It quantifies the total water transport and is especially useful in a comparison of the thermohaline conveyor intensity. At present the northward surface currents carry warm and salty subtropical water far to the north, where it sinks due to surface cooling. The southward currents in the deep ocean deliver cold water to the low latitudes, where it upwells. This meridional motion forms a loop that induces the net northward oceanic heat transport.

Sometimes the overturning stream function itself is referred to as the "conveyor" [e.g., *Boyle and Weaver*, 1994]. However, it is relevant only in describing the zonally averaged circulation. The actual 3–D conveyor is far more complex, as maps of velocity vectors and, especially, the trajectory maps reveal (see below). Nevertheless, the overturning

stream function is critical for our understanding of net mass transport and the salinity conveyor belt operation. First, it shows clearly whether the thermohaline circulation is strong or weak, and second, it readily gives the volume exchange between the low and high latitudes, as well as the deepwater production, the most important climatic indicators.

The overturning stream function in our study appeared to be very similar to that of *Seidov et al* [1996, Figure 5]. Therefore we only briefly describe major features of the overturning pattern without displaying the drawing. The overturning pattern conforms to a simple scheme that closely resembles the general picture of modern meridional overturning which has emerged from numerous computer simulations of different complexity [e.g., *England,* 1993; *Toggweiler et al.,* 1989; *Maier–Reimer et al.,* 1991; *Wright and Stocker,* 1991; *Fichefet et al.*, 1994; *Rahmstorf,* 1994; *Sakai and Peltier,* 1995; *Manabe and Stouffer,* 1995]. Today's forward or clockwise (as seen from the eastern boundary looking west through a vertical plane) gyre of the salinity conveyor occupies most of the ocean from the surface–subsurface layers to a depth of 3 km. This gyre conveys NADW and is thought of as the main wheel of the modern ocean climate. A much weaker abyssal reverse (counterclockwise) gyre conveys AABW (largely in the deepest layer, i.e., below 3 km). Its return (southward) flow joins the southward flow of NADW between 3 and 4 km. In addition, there is a weak, shallow, wind–driven reverse (counterclockwise) gyre in the mid to high latitudes, induced by Ekman convergence in the subtropics.

Note that although glacial NADW production is 8 Sv, much lower than today's value of 13 Sv, the intensity of the glacial conveyor is comparable to that of modern times. If we quantify the southward transport at 30°N, the Upper NADW outflow (see the inventory of the glacial water masses given by, e.g., *Oppo and Lehman* [1993] and *Oppo et al.* [1995]), or forward conveyor branch, does indeed rise to only 8 Sv (1 Sv=$10^6$ $m^3$ $s^{-1}$). However, if we take into account the deep reverse branch comprising AABW and its mixture with Lower NADW still produced in the central northern Atlantic (see below in the discussion of the convection patterns), the total transport amounts to 12 Sv, which gives almost the same intensity of the deep water outflow as the present–day North Atlantic combined deep outflow. The intensity of this depleted of NADW conveyor, similar to present–day conveyor's intensity, is in agreement with the most recent finding based on proxy data analysis [*Yu et al.*, 1996].

As we have already noted, the 3–D conveyor is essentially more complex than its 2–D image given by the total meridional overturning. Figure 2 depicts modern velocity vectors at 50 m and 2000 m. Figure 3 shows the same sequence of maps for the LGM. These maps look similar to those shown by *Seidov et al.* [1996]. For convenience, these maps are also shown here because they are essential for a comparison of the Eulerian and Lagrangian visualization of the simulated currents. One may infer from these figures that the modern and paleo–circulation patterns are indeed very distinct both in the upper and deep ocean. The most noticeable feature is the deviation of the paleo–North Atlantic Drift from its modern northeastern path. Strong zonality of the subpolar front indicates a reduced supply of water that can be downwelled as NADW in the northern North Atlantic and the NGS. Moreover, the route of the return southward flow in the deep ocean changed radically, a robust feature emerging in all our glacial experiments regardless of complexity (compare Figure 2b and Figure 3b). In the eastern part of the basin, the incursion of AABW, seen even in Figure 3b, dominates the near–bed transport up to the Faeroe–Shetland Ridge, in agreement with the water mass contouring by *Sarnthein et al.* [1994]. Hence the redeposited sediment in the eastern mid to high latitudes might be of different origin. Today, the drifts there transport material largely from northeast to west and southwest. In contrast, during the LGM some drifts could change direction of transport to redeposit the grains from south to north and northwest.

Today's southward deep return current is a deep ocean western boundary flow forming a strong countercurrent under the Gulf Stream. This western boundary current is well recognized as the most prominent feature of the thermohaline circulation [*Stommel and Arons,* 1960]. Though a noticeably weaker western boundary current still existed at the LGM, the descending branch returned to the southwestern basin largely as a broad zonal westward flow in the middle latitudes. The glacial countercurrent under the paleo–Gulf Stream was weaker, deeper, and farther eastward. At the LGM a southward deep ocean flow originated near the Rockall Plateau at depth of about 2 km, occurring in the eastern part of the basin, rather than in the western part as today. This particular feature of the computer model in the eastern North Atlantic is again in good agreement with the contouring by *Sarnthein et al.* [1994]. Using the trajectory–tracing model below, we demonstrate that the simulated glacial deep water indeed moved along the eastern flank of the Mid–Atlantic Ridge. Therefore as water in the western deep Atlantic contained more AABW at the LGM, the deep and abyssal water during the glacial time was older than at present.

To understand the mechanism of deep water formation, we investigate changes in the convection regime. The modern deep convection sites are found mainly in the NGS, east and south of Iceland, and in the Labrador Sea. Figure 4a depicts the maximal depths to which convection, induced by hydrostatic instability in the uppermost layer, penetrates. The HM convection pattern is consistent with the patterns given by *Maier–Reimer et al.* [1993], *Toggweiler et al.* [1989], and *Rahmstorf* [1995]. Shallow convection starts in the Gulf Stream area and marks a further progression of subtropical water at high latitudes carried by the North Atlantic Current.

A substantial change in the glacial convection regime is obvious from Figure 4b. The major feature of glacial convection, as compared to its modern state, was the far weaker glacial convection in the NGS and the southward shift of the main convection sites. The maximum ventilation at the LGM occurred in the mid–North Atlantic between 50° and 60°N. This result is well supported by proxy data [*Duplessy et al.,* 1988; *Sarnthein et al.*, 1995]. A southward shift of both the convection sites and the polar front led to a decrease in the northward transport of warm and salty water. Hence a positive feedback worked to establish the glacial mode of circulation. An even farther southward shift of the convection was limited by Ekman pumping in the subtropics which protected the major anticyclonic gyre from shrinking even more, i.e., providing the negative feedback to balance the positive one.

**Sediment accumulation rates and sediment transport.** Total accumulation is governed by the requirement that sources and sinks balance at the sea surface and be the same

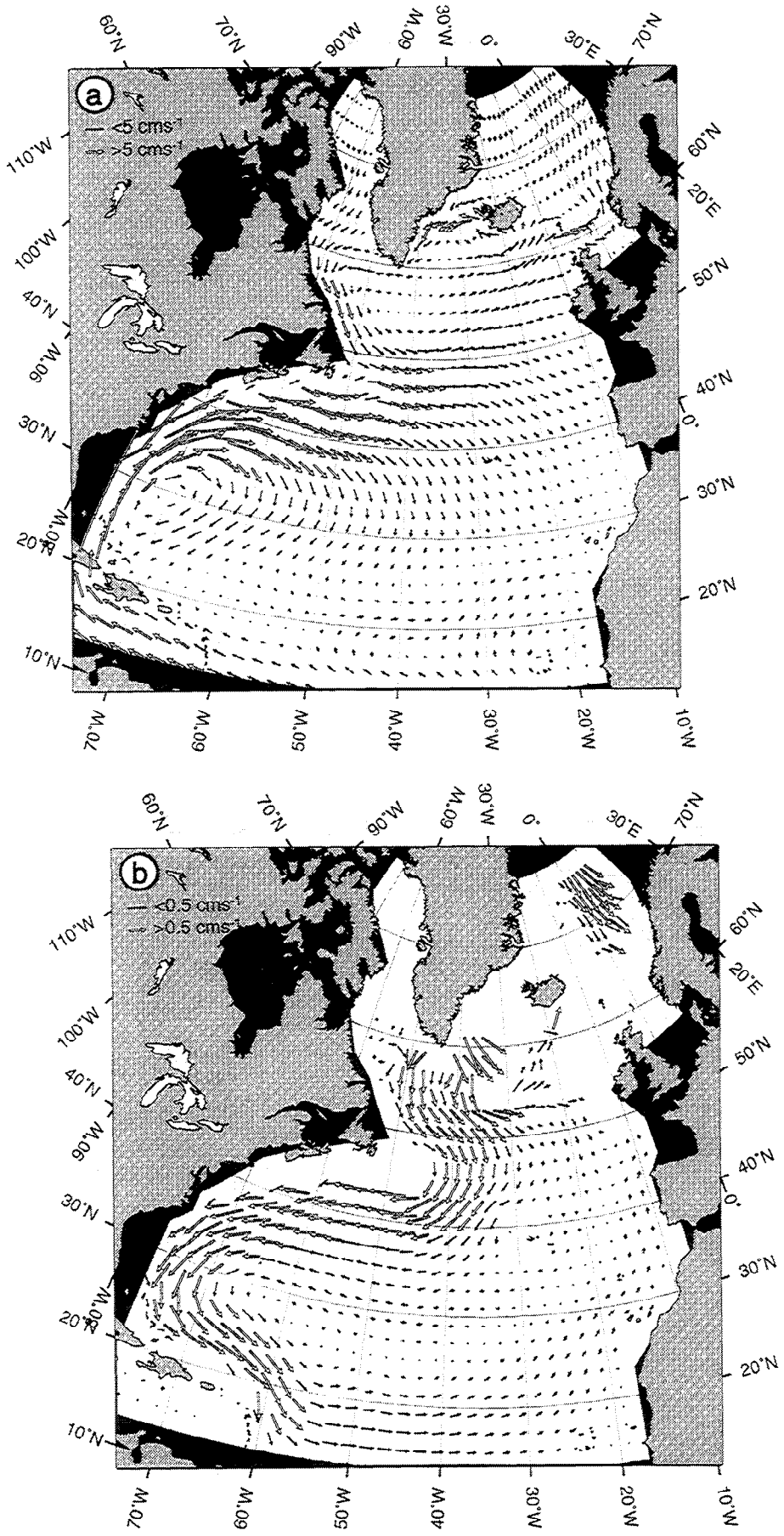


**Figure 2.** Modern velocity (a) at z=50 m and (b) at z=2000 m. The results on 1°x1°, which gives a similar but more detailed distribution of the velocity field, are given by *Seidov et al.* [1996] (see text).

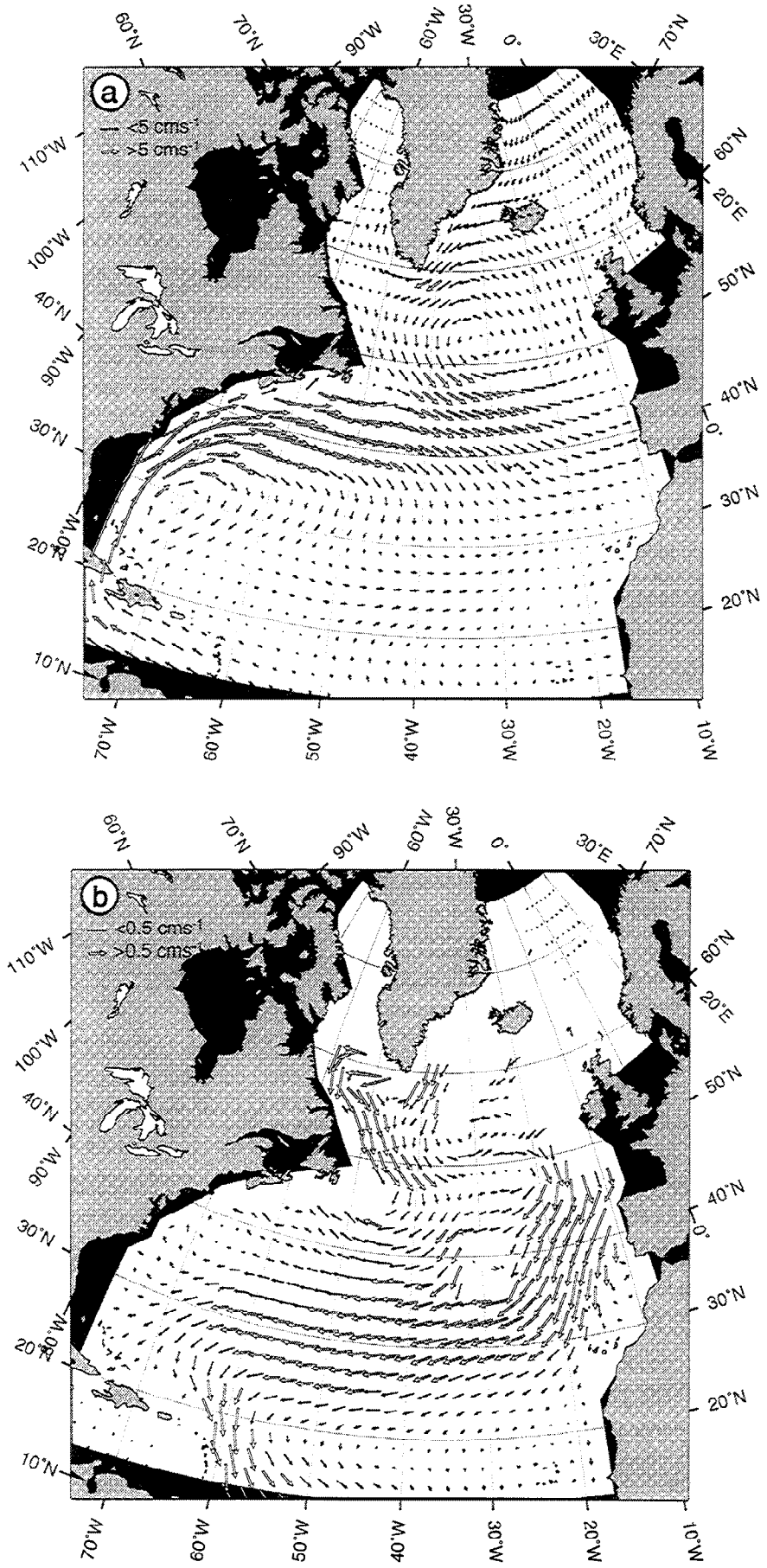


**Figure 3.** LGM velocity (a) at z=50 m and (b) at z=2000 m; (see Figure 2 caption and text).

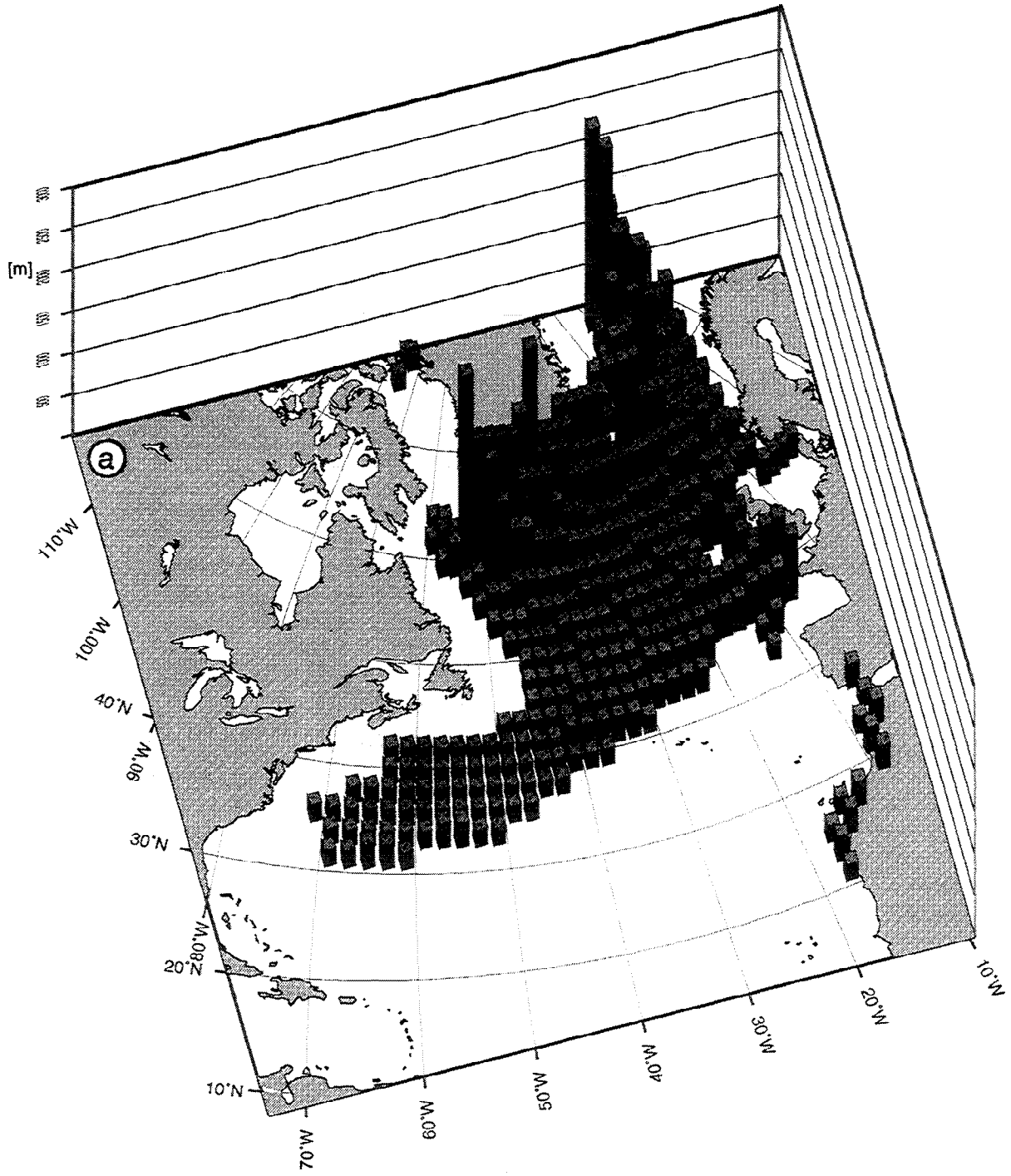


**Figure 4.** Diagrams of convection: (a) the HM and (b) the LGM. The heights of the bars are equal to the depth of convection.

for both time periods. The spatial distribution of sediment is, however, different and reveals two distinctly different circulation modes between present and the LGM. A very high accumulation rate associated with the Holocene/modern mode of circulation is found in the vicinity of Iceland in the Irminger Basin, along the Reykjanes Ridge at both the south and north sides of Iceland, at the Rockall Plateau, and in the NGS (Figure 5a). This is in agreement with the present–day concept of sediment trapping in these areas [*McCave and Tucholke*, 1986; *Bohrmann et al.*, 1990; *Wold*, 1992]. We find that the modeled sediment accumulation rates are smaller than those which have been measured. This is because of the low eolian sediment input from the top and also because of the missing lateral input [*Haupt*, 1995]. The sediment is transported by the deep western southward boundary current with local maxima near Newfoundland and farther to the south in

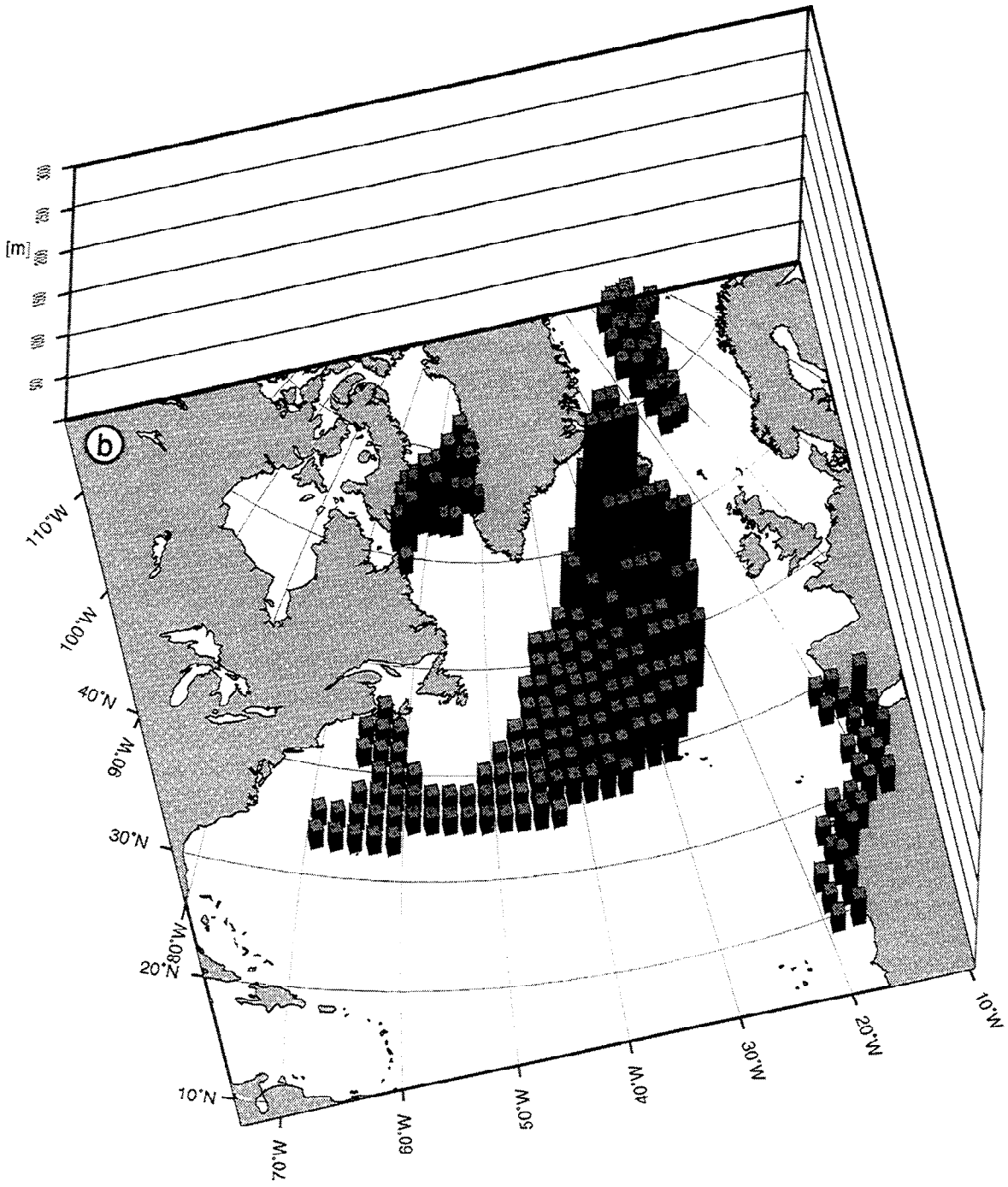


**Figure 4.** (continued)

and near the Caribbean [*McCave and Tucholke*, 1986]. We note that Iceland and the Caribbean are represented by seamounts in the model bottom topography; hence the nonzero accumulation rates are artifacts at the exact positions of these islands.

As the glacial North Atlantic Current diverged from today's north–eastern path, the accumulation rate in the Iceland and Irminger Basins dropped, and most of the sediment mass was spread over the abyssal valley in the Canary Basin (Figure 5b). Note that although the sedimentation rate is far lower there than in the Iceland Basin, the sediment mass is roughly the same because bottom area in the latitude–longitude grid cells increases rapidly to the south. A relatively high glacial accumulation rate is found in the Newfoundland Basin. However, we do not see continuous southward sediment transport along the American coast, a signature of all our experiments based on the modern ocean surface climatology. Instead, a noticeable southward sediment transport is

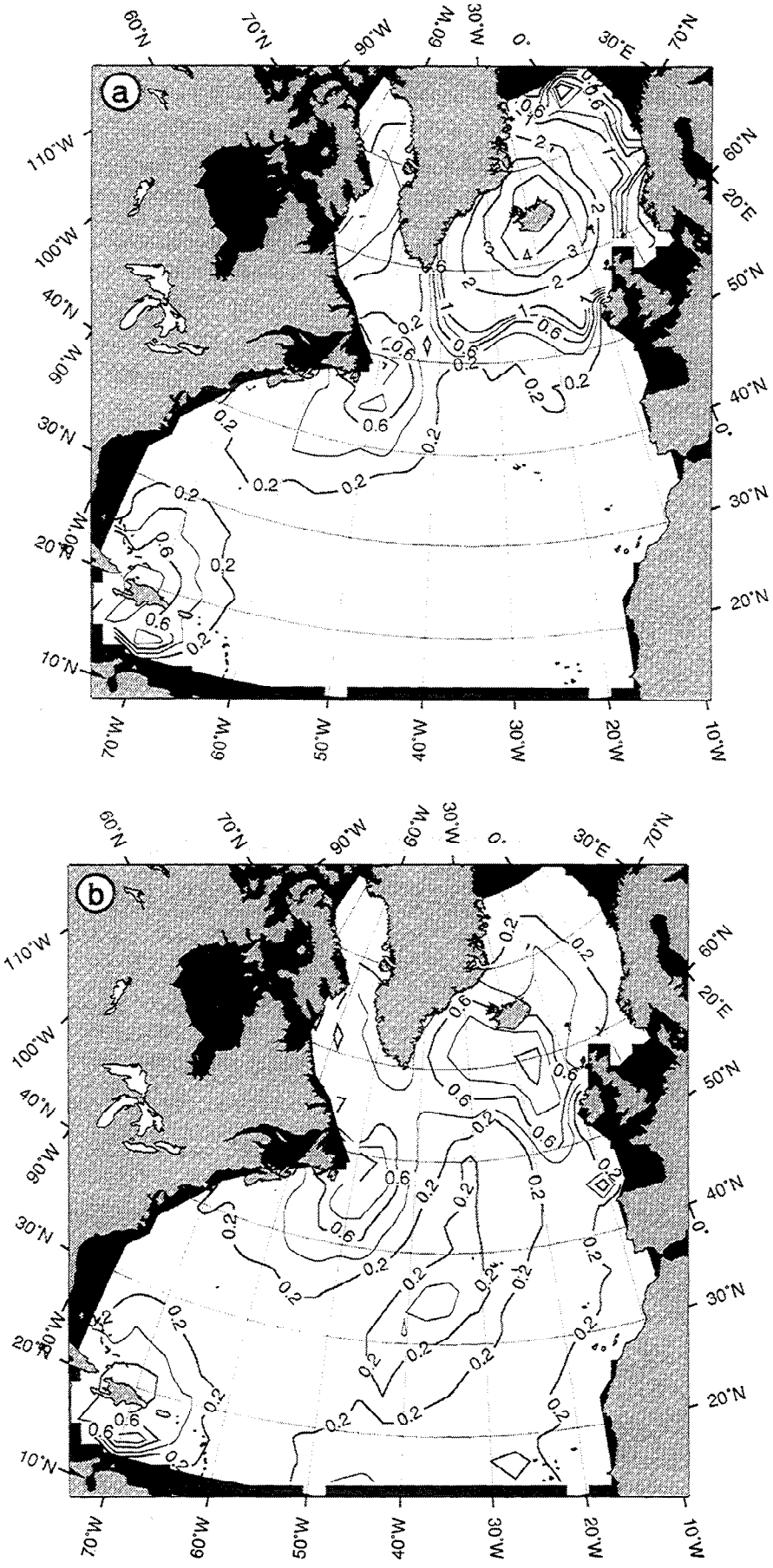


**Figure 5.** Sedimentation rate (centimeters/1000 year) facilitated by (a) the HM and (b) the LGM ocean circulation pattern.

found at the eastern flank of the Mid–Atlantic Ridge, which can be explained by a comparison of Figures 5a and 5b with Figures 2b and 3b.

Though an increased northward incursion of AABW at the LGM in the eastern North Atlantic is consistent with the contouring by *Sarnthein et al.* [1994], the conclusions about an increased reverse abyssal gyre cannot be attributed likewise to the western part of the basin. Indeed, the southward transport, though noticeably curtailed, still existed in the western deep ocean. Velocity maps suggest (and trajectory analysis confirms; see below) that the northward flow of AABW was probably the same as or weaker than today's (Figures 2b and 3b). Simultaneously, the eastern flank of the glacial AABW intrusion (initially through the Vema Fracture Zone) was enhanced considerably. The exchange between the eastern and northern parts of the deep North Atlantic was stronger at the LGM than today.

**Trajectory tracing.** Although most of the features common to the two sediment transport patterns (the modern and the LGM) can be explained by comparing them with the circulation patterns, fundamental differences between glacial and interglacial ventilation and sedimentation regimes are not revealed using solely the velocity maps. The transport in a transit area of intense ventilation can differ principally depending on whether convection is taken into account or ignored. Let us hypothesize that a velocity field is not computed using a prognostic circulation model, but is instead diagnostically calculated from the ocean climatology, e.g., using *Levitus* [1982] data. These climatological fields were formed by all processes including convection. However, the convection is not present in the data directly. Moreover, the convection pattern cannot be reconstructed using this data without running a prognostic model. Hence direct impact of convection on the water motion, it is missed from diagnostic calculations based on these climatological data. In other words, diagnostic velocity would contain no information about convection because hydrostatic instability was removed from the processed climatological data. This means that the Lagrangian particles whose trajectories were calculated on the basis of the observed ocean climatology instead of a prognostic model would drift along the trajectories undisturbed by convection, and therefore these simulated trajectories would be wrong.

*Toggweiler et al.* [1989] show that "robust diagnostic" calculations, in which computed temperature and salinity are restored to observations, fail to reproduce geochemical tracer distributions. On the basis of these results, *Cox* [1989] pointed out that although diagnostic or robust diagnostic thermohaline fields "look" better, the circulation patterns are far superior in prognostic simulations. This may be in part a consequence of radical changes in the circulation patterns induced by convection. The end result for water transport may become rather serious. Indeed, when particles drift into the

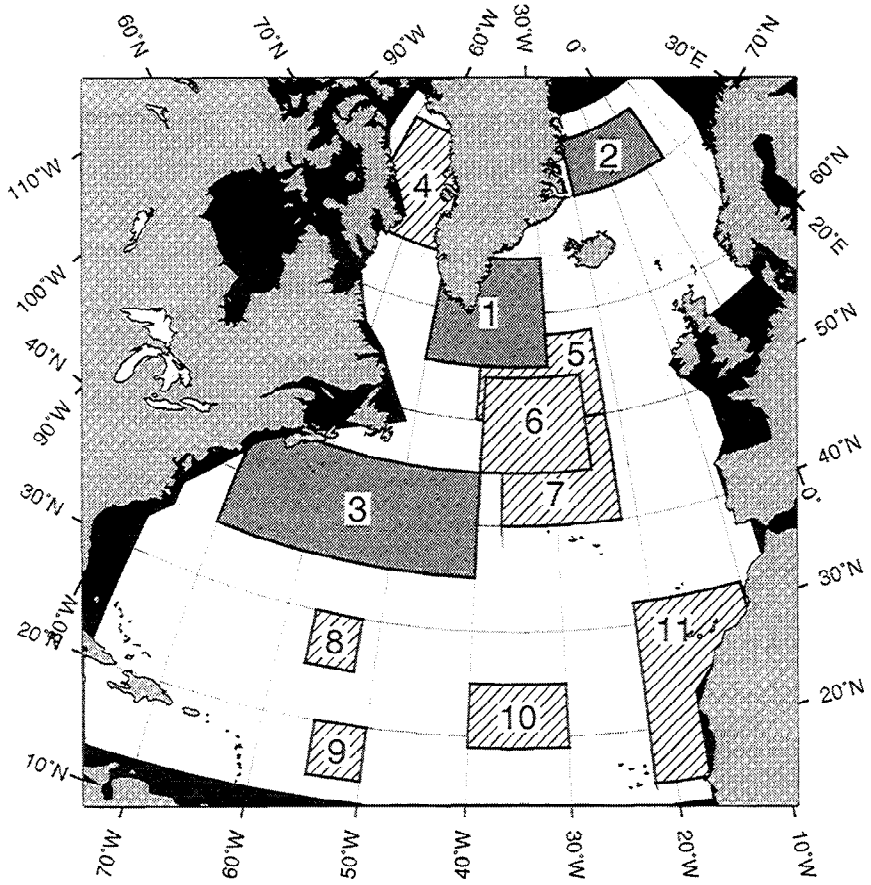


**Figure 6.** Locations of launching of the Lagrangian particles for the 3–D water motion tracing. The particle spaghetti for the particles starting from the shaded areas are shown in Plates 1 and 2.

area where water vigorously mixes vertically, the vertical component of the particle motion may change abruptly. That means the particles may enter a new layer (higher or lower than before mixing) where the currents have a different, possibly even opposite direction.

In our experiments, the particles illustrating the flow were deployed in the areas shown by rectangles in Figure 6. In each of the areas, about 30 particles started to travel through the Eulerian velocity fields, once each in the modern and in the LGM cases. In the following maps (Plates 1 and 2, Figure 7) we employ two different techniques to show the trajectories. In Plates 1 and 2 the trajectories are colored to show the depth of a particle. Plates 1a and 1b are shown to emphasize the role of convection. They delineate the trajectories without the impact of convection over the paths, whereas Plates 1c and 1d illustrate the same time slices but with the impact of convection included (convection sites are depicted by different shades of gray: the deeper the convection, the darker the shade). We use the sunlight spectrum colors, from dark red in the uppermost layer (< 100 m) to violet and black in the two deepest layers, to visualize vertical migration of the water parcels. In contrast, Figure 7 shows the particles' pathways with both depth and elapsed time shown in small rectangles attached to the trajectories (only two pairs of the trajectories are repeated in the black and white Figure 7, namely, those from Plates 1c and 1d, and Plates 2c and 2d). Although the model time in the trajectory–tracing calculations was over 500 years, only the tracks for the first 100–200 years of the elapsed time are shown in the maps to avoid confusion.

A striking feature of the trajectory map is the change in the glacial deep ocean circulation regime which is not so obvious from the velocity maps. This change is far more complex than a simple increase in the zonality of the surface current, a well–known feature of the LGM surface circulation [*CLIMAP,* 1981; *Ruddiman and McIntyre,* 1981; *Kellogg,* 1980]. Though the velocity maps at 2000 m have already displayed rather complicated routes for the deep ocean LGM currents, in contrast to the fairly simple structure of the modern deep flow, only the water volume trajectories reveal the true three–dimensionality of the intermediate to deep flows.

The deep water production at the LGM is found in the model only in the central part of the north central North Atlantic (Plate 1d), which is in agreement with the convection pattern in Figure 4b. We note that water descends in the subpolar gyre in spite of upward motion induced by Ekman divergence. Hence thermohaline currents would drive water along isopycnals in the subsurface layers regardless of ventilating convection; i.e., ventilation of subsurface and intermediate water would occur with, or without, deep convection. The fates of descending volumes are quite different in the cases including convection (Plates 1c and 1d) and those where convection is ignored (Plates 1a and 1b). The pronounced convective chimney forms an intensive cyclonic circulation around a homogenized column of high–density water. As particles deployed at the surface during the LGM became trapped inside this column (Plate 1d), they were propelled downward, forming most of the 8 Sv of glacial NADW (see above). Without convection, most of the particles would be driven out of the cyclonic subgyre and driven into the eastern part of the basin above intermediate depths to enter the NGS, which would contradict the hypothesis that at an intermediate depth there was an outflow from the Nordic Seas over the Faeroe–Shetland Ridge.

Plate 1d indicates that there was some cold intermediate water produced in the NGS at the LGM. This water, flowing farther into the North Atlantic over the Greenland–Iceland sill, was not dense enough to subduct under the intermediate to deep water formed in the central part of the subpolar gyre. It mixed with the subpolar water and stayed at an intermediate depth flowing along the S–shaped route at that depth (bright blue parts of the trajectories in Plates 1d and 2b in the north central part of the basin). Most of the deep return flow occurred along the eastern slope of the Mid–Atlantic Ridge, though some water still contoured the American east coast. In contrast, the water sinking in the NGS today is dense enough to descend even deeper after spilling over the sills into the North Atlantic. Together with the portion of NADW formed east of Greenland and in the Labrador Sea, this water travels southward in the western boundary current comprising most of the 13 Sv of simulated modern NADW outflow shown in Figure 2a. Most of the deep flow contours the American east coast, and a smaller portion is routed along the west slope of the Mid–Atlantic Ridge. We point out that the curtailment of the forward conveyor in the western part of the ocean was not complete. This implies that the conclusions based on analysis of the glacial proxy data assembled along the eastern meridional sections probably are not valid for the western part of the basin.

To conclude the deep circulation description, as inferred from the Lagrangian calculations, we note that the glacial AABW incursion strongly increased as compared to its modern analogue. The sponge layer is employed to restore the numerical solution to the modern deep ocean climatology (note, however, that the impact of the layer is weaker in the upper ocean because of a far longer restoring time in this layer than at the surface; see above). Hence the increased AABW incursion into the abyssal North Atlantic occurs only because of weaker NADW outflow and is not a result of a specified increase of the AABW inflow at the side boundary condition. Note that we do not specify the inflow; an apparent inflow is regulated by restoration to thermohaline conditions at the boundary; e.g., it has the intensity which satisfies the near–climatological distribution of temperature and salinity inside the sponge layer and the circulation in the interior, which is fully prognostic.

We do not try justifying the use of the sponge layer, which is a weak point of any regional study. Yet here the particular result of increased relative importance of AABW sounds realistic. As the sponge layer prescribes, this increase occurred only because the deep western North Atlantic became vacant due to the decreased glacial NADW outflow. Indeed, this strengthening of the reverse abyssal conveyor with the increased role of AABW is the most prominent feature of contoured glacial geochemical tracers in the Atlantic [e.g., *Kroopnick,* 1985; *Sarnthein et al.*, 1994].

In addition to the particles traced from the sea surface, we have deployed trajectories in the deep ocean (areas 7–9 in Figure 6; the trajectory maps are not shown here). The particles illustrating the LGM abyssal flow have longer paths than the particles showing modern flow during the same elapsed

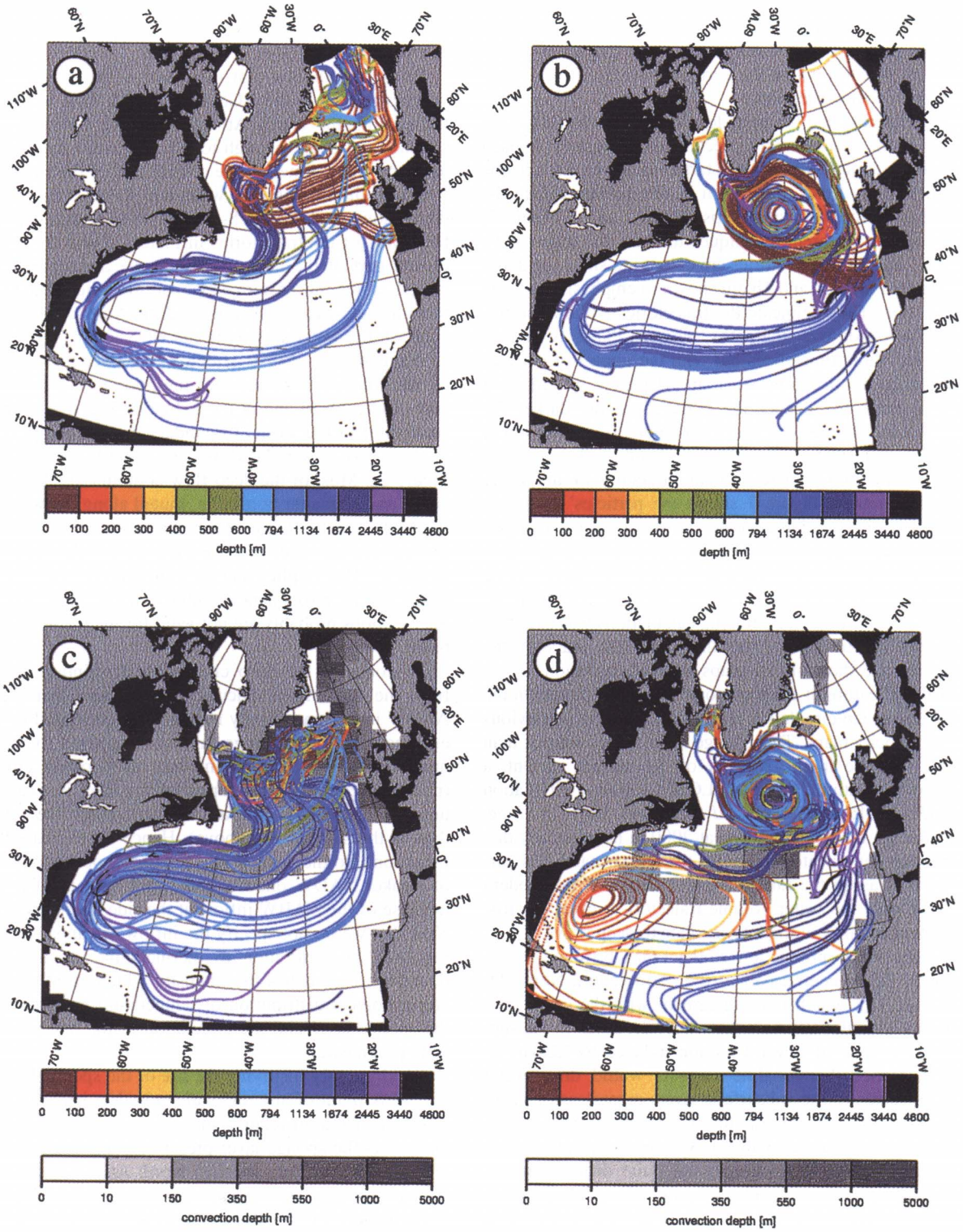


**Plate 1.** Trajectories of particles deployed at the HM in the central part of the northern North Atlantic (area 1 in Figure 6). The top panels show the (a) HM and (b) LGM trajectories calculated without taking into account convection; the bottom panels show the(c) HM and (d) LGM trajectories calculated with the impact of the convection included. The convection depths are shown by different shades of gray (see also Figure 4). The first 100 years of the particles history are shown; as the particle descends or upwells, the color of the trajectory changes.

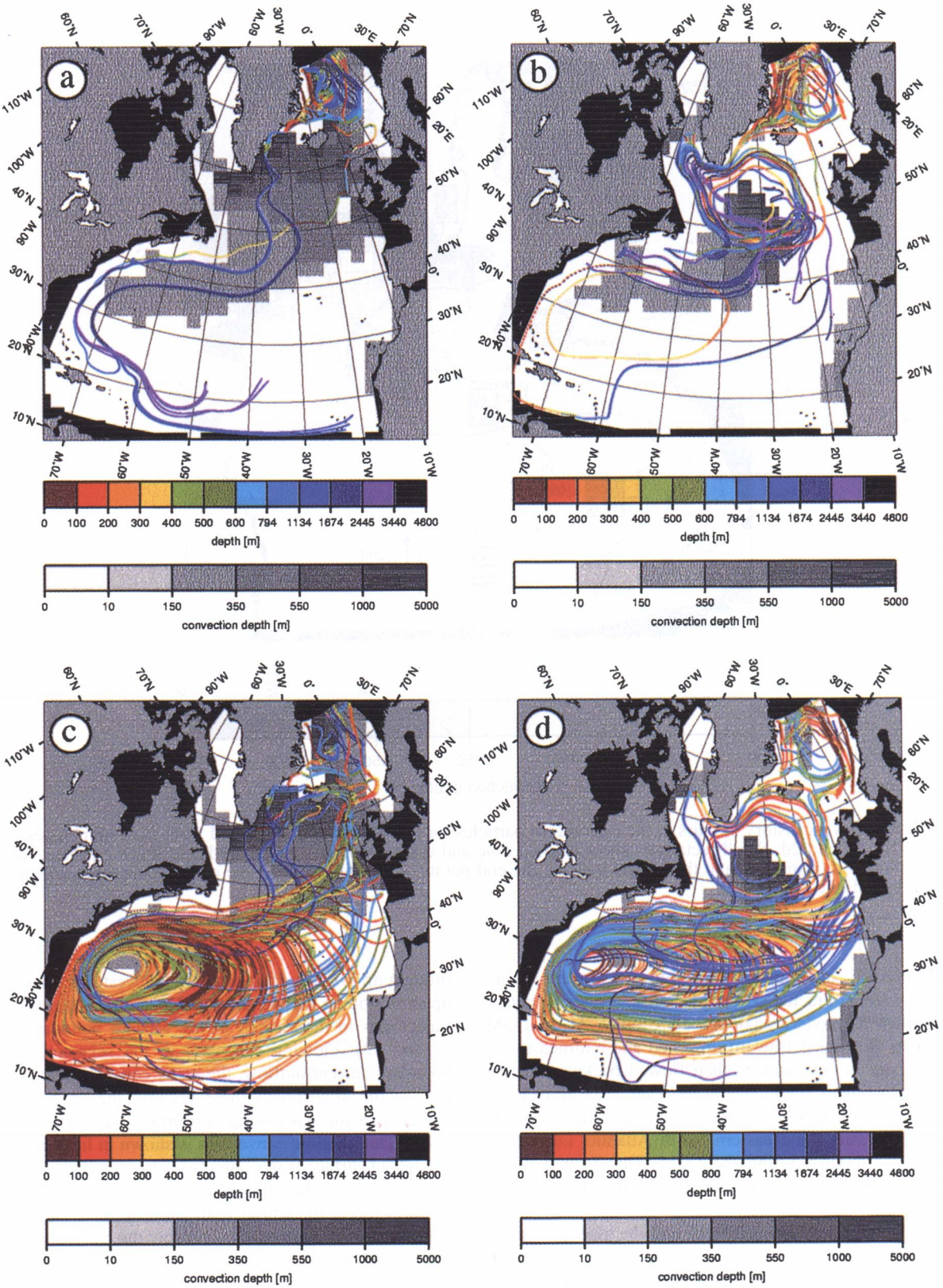


**Plate 2.** Trajectories of particles deployed at the (left) HM and (right) LGM in the Norwegian–Greenland Seas (area 2 in Figure 6) and in the north–western part of subtropical gyre (area 3 in Figure 6). The top panels show the (a) HM and (b) LGM trajectories originating in the NGS; the bottom panels show the (c) HM and (d) LGM trajectories of the particles deployed in the western boundary current outflow. Only the cases with convection included are shown. The convection depths are shown by different shades of gray as in Plate 1. The depth is indicated by colors from the color palette as in Plate 1.

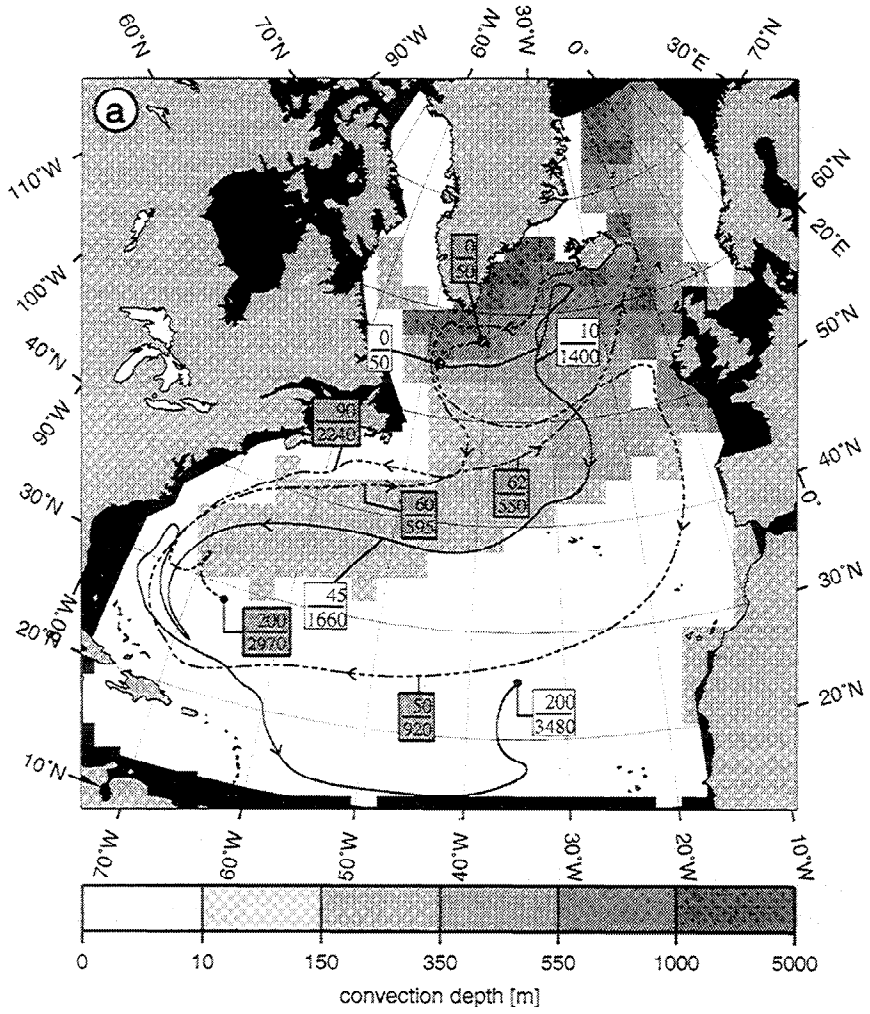


**Figure 7.** A 200–year history of pairs of the Lagrangian particles for (a, c) HM and (b, d) LGM from the assemblages shown in Plates 1c, 1d, 2c, and 2d. Small rectangles show elapsed time and depth, and small circles indicate starting points; the arrows show the direction of motion, and the bullets indicate the end points of the trajectories. One of the trajectories of each pair is presented by a dashed line.

time. Moreover, after penetrating into the eastern basin through the Vema Fracture Zone, glacial flow reached higher latitudes than its modern analogue does today. At the LGM the particles flowing northward upwelled and returned to the western basin. These particles then flowed backward to the eastern basin but in shallower layers. Hence the trajectory–tracing model indicates a vigorous quasi–zonal exchange between the western and eastern North Atlantic, i.e., strong abyssal water mixing during the LGM. This feature is not found in the Lagrangian calculations for the modern time slice.

Plates 1c and 1d compare present and the glacial trajectories' 'spaghetti' in the subtropical anticyclonic gyre. The modern and LGM trajectory maps conform to the Luyten–Pedlosky–Stommel (LPS) ventilated thermocline theory [*Luyten et al.*, 1983] and the computer experiment of *Cox and Bryan* [1984]. The thermocline in the subtropics is maintained by Ekman pumping. Therefore as water circulates in the gyre, it descends and ventilates the thermocline. The water is brought up to subsurface layers in the western boundary along upward sloping isopycnals (orange–colored segments of the trajectories in the vicinity of the western boundary in Plates 2c and 2d). Flowing eastward, in the segment of western boundary current outflow, the water convects because of heat loss to the atmosphere (here because the specified SST is colder than the outflowing subsurface water in this outflow zone). This shallow convection is shown in light gray in Plate 2. The subsurface water parcels in this ventilation zone come in contact with the atmosphere. Then they start to descend again to repeat the whole ventilation cycle. Those water parcels which flow northeastward below the convection depth do not contact the atmosphere again and therefore do not ventilate. Yet, at any given time, new water parcels descend from the surface in the ventilation zone and continue to ventilate. However, the ventilation is restricted to the central and western parts of the gyre. In complete agreement with the LPS theory, there is a shadow zone attached to the eastern boundary, practically unreachable for ventilating volumes. Modern

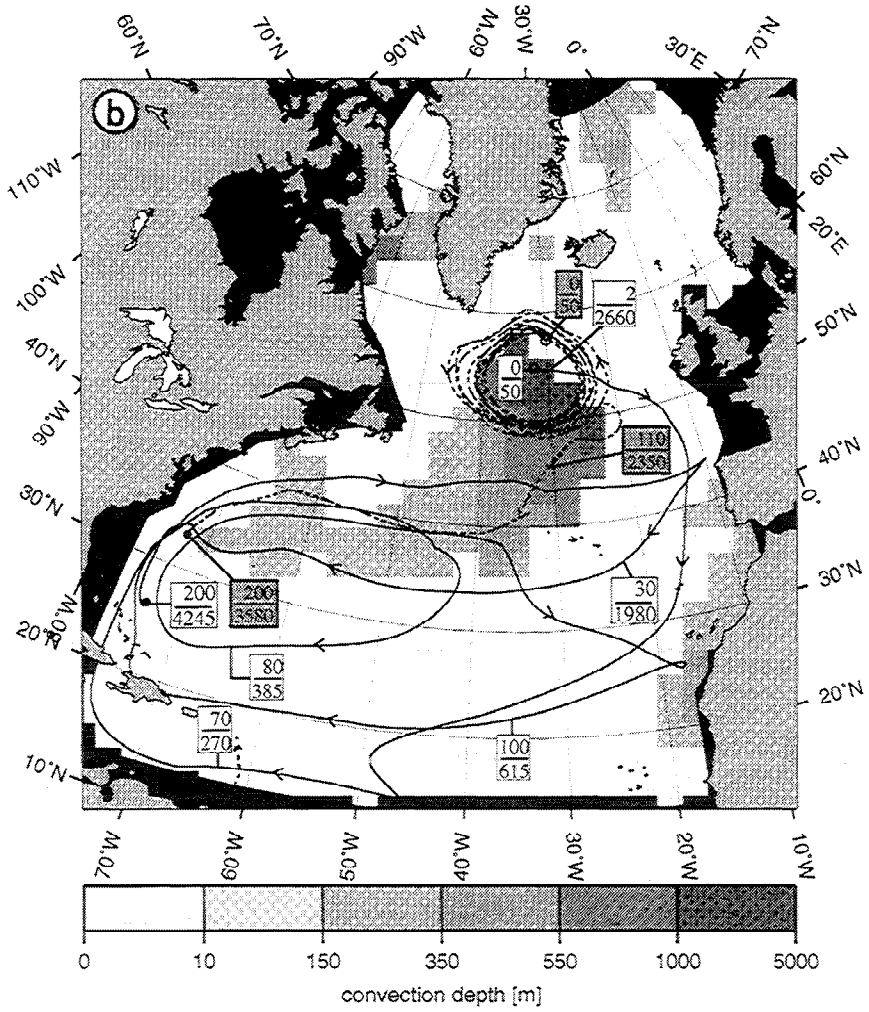


**Figure 7.** (continued)

elapsed times (Plate 2) for a single ventilation cycle in the gyre agree well with the estimates of *Cox and Bryan* [1984]; short loops have an advection age of no more than 3 to 5 years before the water returns to the ventilation zone, whereas the longer paths in the subtropical gyre take more than 10 to 15 years to return to ventilation zone (Plates 2c and 2d, and Figures 7c and 7d). It is obvious from the colors of the trajectories in Plates 2c and 2d that the glacial thermocline is far better (deeper) ventilated than its modern analogue. There is evidence [*Slowey and Curry*, 1992, 1995] that the subtropical thermocline was indeed better ventilated during the last glacial time. As Plate 2d reveals, our Lagrangian calculations agree well with these findings.

Figure 7 indicates that the speed of the particles in the upper and the intermediate layers was not lower at the LGM than today. The deep and abyssal glacial flows, though routed differently from today, were even stronger in the eastern part of the basin. This confirms the concept that the LGM conveyor was at least as intense as the present one [*Yu et al.*, 1996; *Boyle*, 1996]. However, we stress that in contrast to a similar or even higher intensity meridional conveyor at the intermediate depths, the forward conveyor was definitely weaker at the upper to intermediate depths. The most important consequence and indicator of weaker meridional forward upper ocean conveyor is the almost 2 times lower northward heat transport (Table 2). Yet the drop in the heat transport indicates only weakening of the meridional circulation and indicates nothing about the zonal flows. Our analysis of the trajectories provides evidence that zonal flows at the intermediate depths might have been even stronger than today's. On the other hand, the decreased glacial total kinetic energy (Table 2) suggests that generally the glacial circulation was weaker. There are at least two reasons for a decline in the glacial circulation intensity as compared to the modern one. First, the surface and subsurface glacial flows became weaker because of the reduced outflow of the NADW (surface meridional flow is recognized as a water transport that compensates the NADW outflow [e.g., *Schmitz*, 1995]). Second, the deep western boundary current definitely weakened during the LGM due to a reduced shear component in the Gulf Stream

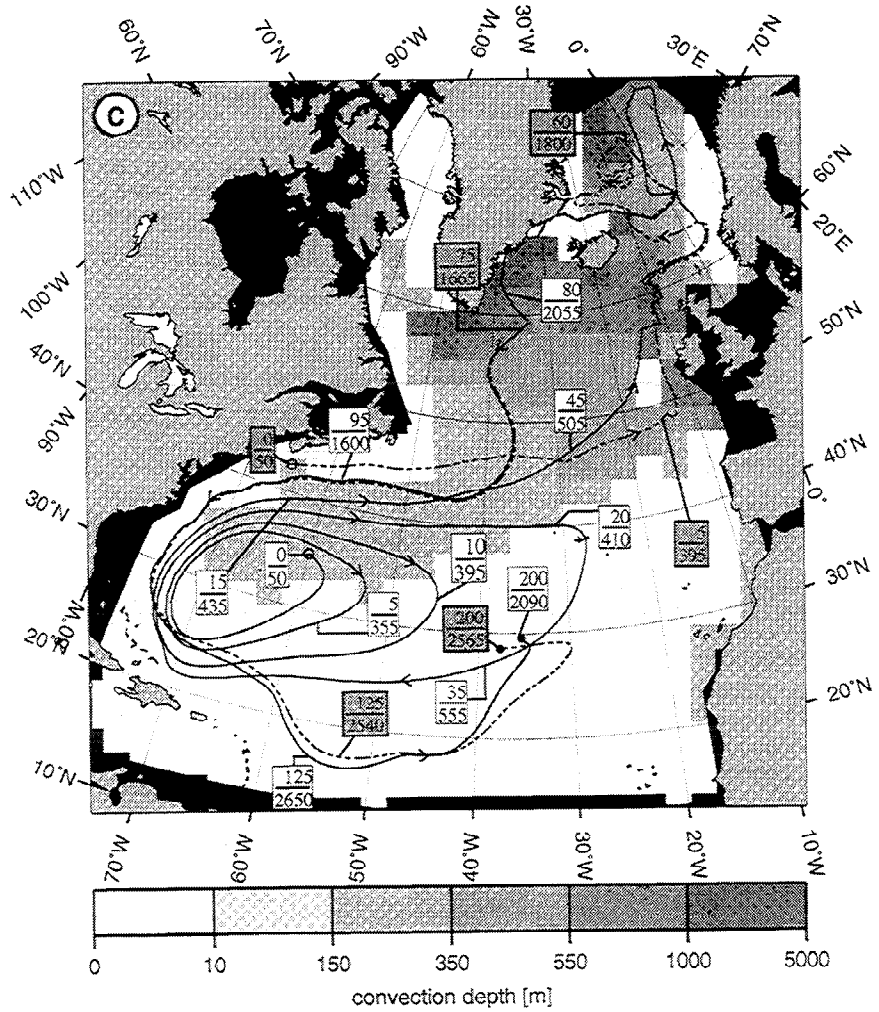


**Figure 7. (continued)**

(this reduction is largely because of a reduced temperature gradient in the western part of a much colder subtropical gyre and, again, reduced NADW production). The competing enhanced inflow of AABW was evidently not energetic enough to compensate for this drop of the forward conveyor intensity and to support the same level of kinetic energy at the LGM as today (Table 2).

## Discussion

A threefold modeling approach was employed to understand particular aspects of the glacial–interglacial change of the North Atlantic circulation which are difficult to address using single-component models. Primary among those are the ventilation regime in the North Atlantic, including the characterization of vertical mixing in convective chimneys and the advective ages of ventilated water. The next intriguing question is whether we can confirm existing inferences about sediment transport and use sediment accumulation as a tool for validation of simulated currents. Circulation studies might focus on the NADW outflow or deep ocean circulation routing. Most of these questions are traditionally addressed using geochemical tracers such as $\delta^{18}O$, $\delta^{13}C$, and $\Delta^{14}C$. The geochemical tracers are extremely useful in the ocean circulation studies and are widely employed. However, the tracers alone cannot provide sufficient constraints over a simulated past circulation, as has been shown recently by *LeGrand and Wunsch* [1995]. In their study they showed that there exist an infinite number of states that would satisfy a tracer distribution aimed at constraining the circulation, at least for the currently available proxy data sets.

Another problem arising in paleoceanographic investigations is the parallel analysis of both surface and the benthic habitats and/or sediment transport features. Commonly, assumed features of a water flow thought to be suitable for explaining a particular distribution of proxy data are largely based on speculations. There is no guarantee that this hypothetical flow would satisfy hydrodynamic restrictions posed over the ocean by the wind stress, ocean geometry, bottom morphology, and sea surface heat and fresh water fluxes. OGCMs may prove a useful addition to analyze the proxy data, having a reasonable and hydrodynamically consistent circulation pattern. Still, it would be better to validate this pattern on the basis of data not used to constrain the condi-

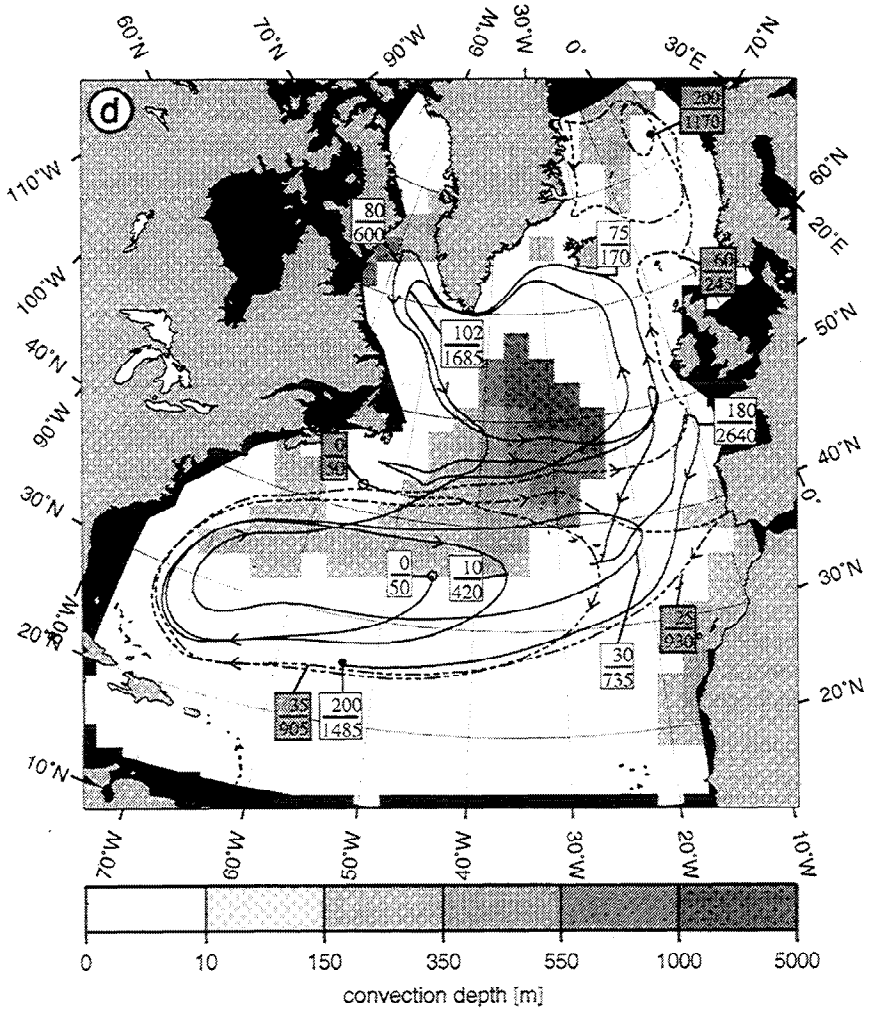


**Figure 7.** (continued)

tions driving the OGCM. Here we employ a sediment transport model to provide such means. Having simulated a sedimentation pattern, one can validate the resulting circulation pattern by comparison with existing interpretations of the sediment structures. As pelagic (and to some extent semipelagic) sediments can be used to verify computations of the modern deep ocean current, they can also be employed to certify paleocirculation.

Based on only partly known SSS, recently corrected SST, and simulated glacial wind stress, our results largely conform to current ideas about ventilation and overturn in the North Atlantic at the height of the last glaciation. The sediment transport model output contains features that agree well with interpretation of sediment data in the northern North Atlantic. *Cremer et al.* [1993] point to a different distribution of sediment during the LGM in spite of the fact that terrigenous fluxes were largely the same as those during the Holocene. They indicate that increased flux along the eastern side of the Mid–Atlantic Ridge is found because of increased bottom current activity in the Feni Drift area. The Feni Drift is the only area with at least undiminished glacial flux. In contrast, the Gardar Drift shows noticeably decreased glacial fluxes, according to *Cremer et al.* [1993]. *McCave and Tucholke* [1986] consider surface and abyssal kinetic energy distribution and net load of suspended sediment in parallel to show that areas of high load are coherent with the maximum of the deep western boundary current. In our experiments, the load along the American east coast is lower during the LGM than today, in agreement with the interpretation given by *Boyle and Keigwin* [1987] on the basis of nutrient concentration analysis. The Caribbean water at depths just above 2 km was nutrient depleted during the glacial period. One interpretation is that there was a lower proportion of northern component water, which in turn means a weaker deep western boundary current and a stronger southern source water incursion.

In the eastern part, our sediment model agrees with data that indicate increased flow along the eastern flank of the Mid–Atlantic Ridge. *Dowling and McCave* [1993] and *Robinson and McCave* [1994] provide evidence that the Feni Drift was substantially enhanced at the last glacial maximum. As in the aforementioned work of *Cremer et al.* [1993], these authors interpret enhanced bottom current activity in the

Rockall Trough region as an indicator of enhanced deep water production there. Our results, indicating a southwest shift of the deep water production from its modern sites (Figure 4), are in good agreement with these findings. Generally, the glacial sediment record indicates an enhanced Holocene bottom current driven by the Iceland–Greenland overflow characteristic of modern NADW production in the Norwegian–Greenland Seas.

Our trajectory–tracing model reveals very different fates of the water volumes in the HM and LGM cases, once exposed to the air–sea interaction and then mixed downward in the convective chimneys. NADW production in the center of the glacial North Atlantic is strongly supported by the proxy data [*Duplessy at al.*, 1988, 1991; *Sarnthein et al.*, 1994, 1995]. In general, the most recent studies indicate enhanced Upper NADW production and decreased Lower NADW production [e.g., *Oppo et al.*, 1995]. However, there exists evidence that, despite decreased Lower NADW production, the glacial conveyor in total was not weaker than today [*Yu et al.*, 1996]. This may appear contradictory to the fact that the glacial northward heat transport was substantially weaker at the LGM. Our trajectory analysis explains this seemingly controversial result. It shows that although the forward conveyor, responsible for meridional heat transport, became weaker, the abyssal reversed branch of the conveyor was enhanced proportionally to support the same intensity of the southward tracer transport in the deep ocean found by *Yu et al.* [1996].

*Duplessy et al.* [1988] argue that during glacial times most of the deep eastern North Atlantic was filled with southern source water which probably penetrated as high as 45°N. Our experiments, deploying particles in the surface layers in the subpolar gyre and in the deep and abyssal areas in the subtropical gyre, are in complete agreement with this conclusion. Moreover, *Michel et al.* [1995] point to a steep gradient in $\delta^{13}C$ distribution northward of 30°N in the North Atlantic delineating the border between southern and northern source water at the LGM. We add that this border probably shifted farther to the north in the eastern part of the basin during that time period.

*Duplessy and Shackleton* [1985] and more recently *Beveridge et al.* [1995] inferred that in the broad time interval of the last 135,000 years, eastern and western parts of the deep North Atlantic were better mixed during glacial periods than today. During warmer times, as today, these parts are well isolated by the Mid–Atlantic Ridge. The trajectory tracing shows that the zonal flows at about 2 km were strongly enhanced during the LGM (the S–shaped circulation developed at intermediate depths instead of the largely meridional flows characteristic of modern circulation; see Figure 3b and Plate 1d). Moreover, the particles deployed in the western abyssal areas (area 8 in Figure 6) showed stronger than modern eastward penetration of the AABW water through the Vema Fracture Zone (Note that this deep ocean channel is somewhat wider in our calculations to allow the water exchange to occur between 10° and 14°N; see the simplified bottom topography in Figure 1). The water penetrating the eastern basin flowed quickly northward and upwelled on its way. As water upwelled, it joined the eastward flowing branch of the S–shaped intermediate to deep current (Figure 4b and Plate 2d). There this water again mixed with AABW and sank to form the complete loop inside the North Atlantic. We are not so certain about the relevance of the behavior just near the southern border because of the sponge layer's influence. Yet this scheme seems to agree with the arguments of *Duplessy and Shackleton* [1985] and *Beveridge et al.* [1995] about enhanced mixing between western and eastern abyssal parts of the North Atlantic during glacial periods. Between 2 km and the bottom in the abyssal gap representing the Vema Fracture Zone the eastward transport increased from less than 1 Sv at present to more than 3 Sv at the LGM.

Finally, we point out that the trajectory analysis is in agreement with the notion of a far better ventilated and deeper glacial thermocline in the subtropical North Atlantic [*Slowey and Curry*, 1995]. These authors provide the data analysis that indicates that the glacial thermocline was shallower than today with its base raised by about 100 m. However, the water inside the glacial thermocline was up to 4°C cooler than today. Our Plate 2 confirms that the glacial thermocline was better ventilated and that there was an enhanced production of subtropical mode water. Deeper glacial ventilation, evident in Plate 2d, implies that the base of thermocline had to rise upward because water pumped into the thermocline was more than 4°C colder at the glacial ventilation points (westward boundary outflow region; compare Plates 2c and 2d). To quantify this effect, the difference between today's and the LGM simulated temperature is shown in a meridional section of the temperature anomaly field in Figure 8. In essence, Figure 8 displays a penetration of cold anomalies deep into the thermocline. It is clear, however, that this penetration is limited to the upper 1 km and that the lower 500 m of this layer is more strongly cooled down than the upper 500 m. This implies that the thermocline base has been raised. A comparison of the temperature profiles in the subtropical gyres indicates that on average the thermocline depth was about 200 m shallower than today, which differs from the estimates of *Slowey and Curry* [1995]. There may be several reasons for this discrepancy. First, the subtropical gyre is dangerously close to the sponge layer at the southern wall, which might have dis-

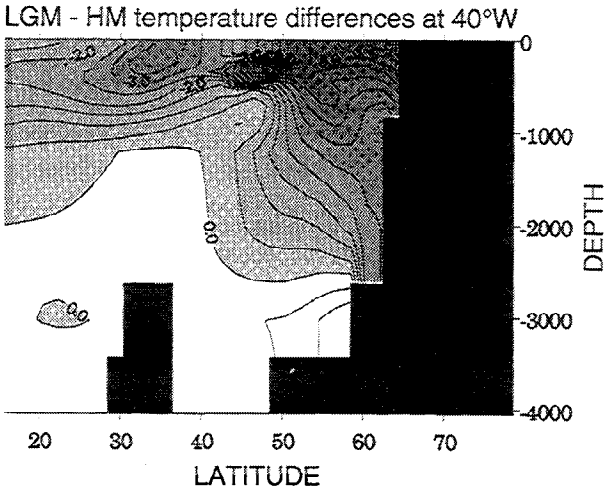


**Figure 8.** Temperature differences (LGM–HM) at the meridional section at 40°W. The sponge layer from 10°N to 16°N is masked. Areas of negative values are shaded.

torted the behavior of the thermocline base. Second, we use the annual mean surface forcing and, therefore, we are unable to simulate an extreme winter southward migration of the density outcrop intersecting the Ekman pumping within the subtropical gyre. Nevertheless, the general tendencies sketched in Figure 1 of *Slowey and Curry* [1995, p. 717] are evident in our trajectory maps (Plate 2d as compared to Plate 2c). The particles dive deeper into the thermocline and stay there longer. The northern limit of the subtropical gyre, marked by the shallow convection along the North Atlantic Drift, is shifted noticeably southward.

As some findings have indicated [e.g., *Sarnthein et al.*, 1995], the Nordic Seas were more isolated from the northern North Atlantic at the LGM than today. This is strongly supported by our Lagrangian calculations. As Figure 7 displays, the water from the subtropics probably had a very limited chance to enter the Nordic Seas, largely because the outflow over the Iceland–Greenland Ridge was reduced during the LGM (Plates 2a and 2b).

## Conclusions

Based on a threefold numerical simulation of the North Atlantic circulation and sedimentation we draw the following conclusions:

1. The North Atlantic circulation and the regime of deep water formation were different at the Holocene/modern and at the LGM time slices. Both ventilation and deep circulation patterns indicate that major changes occurred in the intermediate to deep water layers because of the south westward shift of the convection sites at the LGM relative to the present. The glacial deep convection occurred only in the center of the subpolar gyre, with a very small portion of somewhat shallower convection found to the north of 60°N. Nonetheless, the glacial conveyor appeared to be still rather intensive, yet it was noticeably depleted in NADW. *Seidov et al.* [1996] show that the simulated NADW outflow was only 8 Sv at the LGM, much lower than today's simulated value of 13 Sv. However, the trajectory–tracing model indicates strongly changed routes of deep flows.

2. Sedimentation in the North Atlantic is nonlinearly coupled to the circulation modes associated with different surface climatology. The LGM sedimentation pattern differs fundamentally from the Holocene/modern pattern and in a way that cannot be expected a priori. The major differences indicated by sediment transport and trajectory–tracing models are summarized in following conclusions.

3. Glacial sedimentation rates in the area of the most intense modern sediment deposition are relatively low. The sediment load in the western part of the basin confirms a weakening of the deep western boundary current at the LGM.

4. The LGM sediment rate distribution indicates an enhanced incursion of the AABW in the eastern abyssal part of the basin. However, the curtailment of the forward conveyor in the western part of the ocean was not complete. This implies that the conclusions based on the analysis of glacial proxy data assembled along the eastern meridional sections are probably invalid for the western part of the basin. In agreement with proxy data indications, our Lagrangian calculations reveal far stronger water exchange in the deep ocean between the western and the eastern parts of the basin during the LGM, in sharp contrast with the pronounced isolation of these regions today. The velocity fields in the area of the Vema Fracture Zone show increase of the eastward transport between 2 km and the bottom from less than 1 Sv at present to more than 3 Sv at the LGM.

5. The trajectory–tracing model indicates far stronger ventilation of the thermocline in the glacial low latitudes than is observed today.

6. Concerning the use of numerical models as a principal source of sediment transport and Lagrangian calculations, it should be stressed that at high latitudes the sediment transport and water–volume tracing models can only operate with the simulated rather than observed circulation patterns. The water transport calculations depend critically on knowledge about where the convection occurs and how deep it ventilates. Hence, the velocity patterns and/or thermohaline patterns alone cannot provide adequate information for a particle transport model. This is a very unusual situation in which simulations, rather than observations, can be a source of information for other models.

**Acknowledgments.** The authors gratefully acknowledge the help and support given by Michael Sarnthein and Karl Stattegger. We are thankful to Ralf Prien and to Michael Schulz for their help and fruitful discussions. We are very grateful to Erika Dade and Avan Antia who have corrected our numerous language errors. The authors thank Ernst Maier–Reimer, an anonymous reviewer, and the Editor for very useful comments and suggestions which led to substantial improvement of the manuscript. This study was supported by the Deutsche Forschungsgemeinschaft (DFG) within the framework of the SFB 313 at Kiel University (SFB 313 Project B4) and by the German National Program of Climate Research.

## References

Beveridge, N. A. S., H. Elderfield, and N. J. Shackleton, Deep thermohaline circulation in the low–latitude Atlantic during the last glacial, *Paleoceanography, 10*, 643–660, 1995.

Bitzer, K., and R. Pflug, DEPOD: A three–dimensional model for simulating clastic sedimentation and isostatic compensation in sedimentary basin, in *Quantitative Dynamics Stratigraphy*, edited by T. A. Cross, pp. 335–348, Prentice Hall, New York, 1990.

Bohrmann, G., R. Henrich, and J. Thiede, Miocene to Quaternary paleoceanography in the northern North Atlantic: Variability in carbonate and biogenic opal accumulation, in *Geological History of the Polar Oceans: Arctic Versus Antarctic*, edited by U. Bleil and J. Thiede, pp. 647–675, Kluwer Acad., Norwell, Mass., 1990.

Bond, G. C., Climate and conveyor, *Nature, 377*, 383–384, 1995.

Bond, G.et al., Evidence for massive discharges of icebergs into the North Atlantic Ocean during the last glacial period, *Nature, 360*, 245–249, 1992.

Böning, C. W., and M. D. Cox, Particle dispersion and mixing of conservative properties in an eddy–resolving model, *J. Phys. Oceanogr., 18*, 320–338, 1988.

Böning, C. W., R. Döscher, and R. G. Budich, Seasonal transport in the western North Atlantic: Experiments with an eddy–resolving model, *J. Phys. Oceanogr., 21*, 1271–1289, 1991.

Boyle, E., Deep water distillation, *Nature, 379*, 679–680, 1996.

Boyle, E. A., and L. D. Keigwin, North Atlantic thermohaline circulation during the past 20,000 years linked to high–latitude surface temperature, *Nature, 330*, 35–40, 1987.

Boyle, E., and A. Weaver, Conveying past climates, *Nature, 372*, 41–42, 1994.

Broecker, W., The great ocean conveyor, *Oceanography, 4*, 79–89, 1991.

Broecker, W. S., and G. H. Denton, The role of ocean atmosphere reorganizations in glacial cycles, *Geochim. Cosmochim. Acta, 53*, 2465–2501, 1989.

Bryan, F., High–latitude salinity effects and interhemispheric thermohaline circulations, *Science, 323*, 301–304, 1986.

Bryan, F., Parameter sensitivity of primitive equation ocean general circulation models, *J. Phys. Oceanogr., 17*, 970–985, 1987.

Bryan, F., and W. Holland, A high resolution simulation of the wind– and themohaline–driven circulation in the North Atlantic Ocean, in *Parameterization of Small–Scale Processes*, edited by P. Müller and D. Henderson, pp. 99–115, Hawaii Inst. of Geophys., Honolulu, 1989.

Bryan, K., A numerical method for the study of the circulation of the world ocean, *J. Comput. Phys., 4*, 347–376, 1969.

Climate: Long–Range Investigation Mapping and Prediction (CLIMAP) Project Members, Seasonal reconstructions of the Earth's surface at the last glacial maximum, *Map and Chart Ser. MC–36*, pp. 1–18, Geol. Soc. of Am., Boulder, Colo., 1981.

Colin de Verdière, A., Buoyancy driven planetary flows, *J. Mar. Res., 46*, 215–265, 1988.

Cox, M. D., A primitive equation, 3–dimensional model of the ocean, Tech. Rep. No. 1, 250 pp., Ocean Group, Geophys. Fluid Dyn. Lab., Princeton, Univ., Princeton, N.J., 1984.

Cox, M., An idealized model of the world ocean, I, The global–scale water masses, *J. Phys. Oceanogr., 19*, 1730–1752, 1989.

Cox, M., and K. Bryan, A numerical model of the ventilated thermocline, *J. Phys. Oceanogr., 14*, 674–687, 1984.

Cremer, M., J.–C. Faugeres, F. E. Grousset, and E. Gonthier, Late Quaternary sediment flux on sedimentary drifts in the northeast Atlantic, *Sediment. Geol., 82*, 89–101, 1993.

Dowling, L. M., and I. N. McCave, Sedimentation on the Feni drift and late Glacial bottom water production in the northern Rockall Trough, *Sediment. Geol., 1993*, 79–87, 1993.

Duplessy, J.–C., and N. J. Shackleton, Response of global deep–water to Earth's climate change 135,000–107,000 years ago, *Nature, 316*, 500–507, 1985.

Duplessy, J.–C., N. J. Shackleton, R. G. Fairbanks, L. Labeyrie, D. Oppo, and N. Kallel, Deepwater source variations during the last climatic cycle and their impact on the global deepwater circulation, *Paleoceanography, 3*, 343–360, 1988.

Duplessy, J.–C., L. Labeyrie, A. Julliet–Lerclerc, J. Duprat, and M. Sarnthein, Surface salinity reconstruction of the North Atlantic Ocean during the last glacial maximum, *Oceanol. Acta, 14*, 311–324, 1991.

England, M. H., Representing global–scale water masses in ocean general circulation models, *J. Phys. Oceanogr., 23*, 1523–1552, 1993.

Fichefet, T., and S. Hovine, The glacial ocean: A study with a zonally averaged, three–basin ocean circulation model, in *Ice in Climate System, NATO ASI Ser., Ser. I*, 12, edited by W. R. Peltier, pp. 433–458, Springer–Verlag, New York, 1993.

Fichefet, T., S. Hovine, and J.–C. Duplessy, A model study of the Atlantic thermohaline circulation during the last glacial maximum, *Nature, 372*, 252–255, 1994.

Goldschmidt, P., Accumulation rates of coarse–grained terrigenous sediment in the Norwegian–Greenland Sea: Signals of continental glaciation, *Mar. Geol., 128*, 137–151, 1995.

Goldschmidt, P. M., S. Pfirmann, I. Wollenburg, and R. Henrich, Origin of sediment pellets from the Arctic seafloor. Sea ice or icebergs?, *Deep Sea Res., 372*, 252–255, 1992.

Gordon, A., Interocean exchange of thermocline water, *J. Geophys. Res., 91*, 5037–5046, 1986.

Gordon, A. L., S. E. Zebiak, and K. Bryan, Climate variability and the Atlantic Ocean, *Eos Trans. AGU, 73*, 161, 164–165, 1992.

Hasselmann, K., An ocean model for climate variability studies, *Prog. in Oceanogr., 11*, 69–92, 1982.

Haupt, B. J., Numerische Modellierung der Sedimentation im nördlichen Nordatlantik, *Ber. 54*, pp. 1–129, Sonderforschungsbereich 313, Univ. Kiel, Kiel, Germany, 1995.

Haupt, B. J., C. Schäfer–Neth, and K. Stattegger, Modeling sediment drifts: A coupled oceanic circulation–sedimentation model of the northern North Atlantic, *Paleoceanography, 9*, 897–916, 1994.

Haupt, B. J., C. Schäfer–Neth, and K. Stattegger, Three–dimensional numerical modeling of late Quaternary paleoceanography and sedimentation in the northern North Atlantic, *Geol. Rundsch., 84*, 137–150, 1995.

Honjo, S., Particle fluxes and modern sedimentation in the polar oceans, in *Polar Oceanography*, Part B, edited by W. O. Smith, pp. 687–739, Academic, San Diego, Calif., 1990.

Keigwin, L. D., G. Jones, and S. J. Lehman, Deglacial meltwater discharge, North Atlantic deep circulation, .and abrupt climate change, *J. Geophys. Res., 96*, 16811–16826, 1991.

Kellogg, T. B., Paleoclimatology and paleo–oceanography of the Norwegian and Greenland Seas; Glacial–interglacial contrasts, *Boreas, 9*, 115–137, 1980.

Killworth, P. D., Deep convection in the world ocean, *Rev. Geophys., 21*, 1–26, 1983.

Kroopnick, P. M., The distribution of $^{13}C$ and $\Sigma CO_2$ in the world oceans, *Deep Sea Res., 32*, 57–84, 1985.

Lautenschlager, M., and K. Herterich, Atmospheric response to ice age conditions — Climatology near the Earth's surface, *J. Geophys. Res., 95*, 22,547–22,557, 1990.

LeGrand, P., and K. Wunsch, Constraints from paleotracer data on the North Atlantic circulation during the last glacial maximum, *Paleoceanography, 10*, 1011–1045, 1995.

Lehman, S. J., and L. D. Keigwin, Sudden changes in North Atlantic circulation during the last deglaciation, *Nature, 356*, 757–762, 1992.

Levitus, S., Climatological atlas of the world ocean, *NOAA Prof. Pap., 13*, 173 pp., U.S. Govt. Print. Off., Washington, D.C., 1982.

Levitus, S., and T. P. Boyer, *World Ocean Atlas 1994*, vol. 4, (Temperature; 117 pp.), NOAA Natl. Environ. Satell. Data and Inf. Ser., Washington, D.C., 1994.

Levitus, S., R. Burgett, and T. P. Boyer, *World Ocean Atlas 1994*, vol.3, (Salinity; 99 pp.) NOAA Natl. Environ. Satell. Data and Inf. Ser., Washington, D.C., 1994.

Lorenz, S., B. Grieger, P. Helbig, and K. Herterich, Investigating the sensivity of the atmospheric general circulation Model ECHAM 3 to paleoclimate boundary conditions, *Geol. Rundsch., 85*, 513–524, 1996.

Luyten, J. R., J. Pedlosky, and H. Stommel, The ventilated thermocline, *J. Phys. Oceanogr., 13*, 292–309, 1983.

Maier–Reimer, E., and U. Mikolajewicz, Experiments with an OGCM on the cause of the Younger Dryas, *Rep. 39*, 13 pp., Max–Plank–Inst. für Meteorol., Hamburg, Germany, 1989.

Maier–Reimer, E., U. Mikolajewicz, and K. Hasselmann, On the sensitivity of the global ocean circulation to changes in the surface heat flux forcing , *Rep. 68*, 67 pp., Max–Plank–Inst. für Meteorol., Hamburg, Germany, 1991.

Maier–Reimer, E., U. Mikolajewicz, and K. Hasselmann, Mean circulation of the Hamburg LSG OGCM and its sensitivity to the thermohaline surface forcing, *J. Phys. Oceanogr., 23*, 731–757, 1993.

Manabe, S., and R. J. Stouffer, Two stable equilibria of a coupled ocean–atmospher model, *J. Clim., 1*, 841–866, 1988.

Manabe, S., and R. J. Stouffer, Simulation of abrupt change induced by freshwater input to the North Atlantic Ocean, *Nature, 378*, 165–167, 1995.

Marotzke, J., and J. Willebrand, Multiple equilibria of the global thermohaline circulation, *J. Phys. Oceanogr., 21*, 1372–1385, 1991.

Maslin, M. A., N. J. Shackleton, and U. Pflaumann, Surface water temperature, salinity, and density changes in the northeast Atlantic during the last 45,000 years: Heinrich events, deep water formation, and climatic rebounds, *Paleoceanography, 10*, 527–544, 1995.

McCartney, M. S., Recirculating components to the deep boundary current of the nothern North Atlantic, *Prog. in Oceanogr., 29*, 283–383, 1992.

McCave, I. N., and B. E. Tucholke, Deep current controlled seimentation in the western North Atlantic, in *The Geology of North America*, vol. M. *The Western North Atlantic Region*, edited by P. R. Vogt and B. E. Tucholke, pp. 451–468, Geol. Soc. of Am., Boulder, Colo., 1986.

Michel, E., L. D. Labeyrie, J.-C. Duplessy, N. Gorfti, M. Labracherie, and J.-L. Turon, Could deep Subantarctic convection feed the world deep basins during the last glacial maximum?, *Paleoceanography*, *10*, 927–942, 1995.

Mikolajewicz, U., A meltwater induced collapse of the 'conveyor belt' themohaline circulation and its influence on the distribution of $\Delta^{14}C$ and $\delta^{18}O$ in the oceans, *Rep. 189*, 25 pp., Max–Plank–Inst. für Meteorologie, Hamburg, Germany, 1996.

Miller, M. C., I. N. McCave, and P. D. Komar, Threshold of sedimentation under unidirectional currents, *Sedimentol.*, *24*, 507–528, 1977.

Oppo, D. W., and S. J. Lehman, Mid–depth circulation of the subpolar north Atlantic during the last glacial maximum, *Science*, *259*, 1148–1152, 1993.

Oppo, D. W., M. E. Raymo, G. P. Lohmann, A. C. Mix, J. D. Wright, and W. L. Prell, A $\delta^{13}C$ record of Upper North Atlantic Deep Water during the past 2.6 million years, *Paleoceanogr.*, *10*, 373–394, 1995.

Pacanowski, R., K. Dixon, and A. Rosati, The GFDL modular ocean users guide, *Tech. Rep. 2*, Ocean Group, Geophys. Fluid Dyn. Lab., Princeton Univ., Princeton, N. Y., 1993.

Pfirmann, S., M. A. Lange, I. Wollenburg, and P. Schlosser, Sea ice characteristics and the role of sediment inclusions in deep–sea deposition: Arctic – Antarctic comparisons, in *Geological History of the Polar Oceans: Arctic Versus Antarctic*, edited by U. Bleil and J. Thiede, pp. 187–211, Kluwer Acad., Norwell, Mass., 1990.

Puls, W., Numerical simulation of bedform mechanics. Mitteilungen des Inst. für Meeresk. Univ. Hamburg, Hamburg, Germany, 147 pp., 1981.

Rahmstorf, S., Rapid climate transitions in a coupled ocean–atmosphere model, *Nature*, *372*, 82–85, 1994.

Rahmstorf, S., Bifurcations of the Atlantic thermohaline circulation in response to changes in the hydrological cycle, *Nature*, *378*, 145–149, 1995.

Robinson, S. G., and I. N. McCave, Orbital forcing of bottom–current enhanced sedimentation on Feni Drift, NE Atlantic, during the mid–Pleistocene, *Paleoceanography*, *9*, 943–972, 1994.

Ruddiman, W. F., and A. McIntyre, The mode and mechanism of the last deglaciation: Oceanic evidence., *Quat. Res.*, *16*, 125–134, 1981.

Sakai, K., and W. R. Peltier, A simple model of the Atlantic thermohaline circulation: Internal and forced variability with paleoclimatological implications, *J. Geophys. Res.*, *100*, 13,455–13,479, 1995.

Sarmiento, J. L., On the north and tropical Atlantic heat balance, *J. Geophys. Res.*, *91*, 11,677–11,689, 1986.

Sarnthein, M., K. Winn, S. J. A. Jung, J.-C. Duplessy, L. Labeyrie, H. Erlenkeuser, and G. Ganssen, Changes in east Atlantic deepwater circulation over the last 30,000 years — eight time slice reconstructions, *Paleoceanography*, *9*, 209–267, 1994.

Sarnthein, M. et al., Variations in Atlantic Ocean paleoceanography, 50°–80°N: A time slice record of the last 30,000 years, *Paleoceanography*, *10*, 1063–1094, 1995.

Schmitz, W. J., Jr., On the interbasin–scale thermohaline circulation, *Rev. Geophys.*, *33*, 151–173, 1995.

Schulz, H., Meeresoberflächentemperaturen im frühen Holozän 10,000 Jahre vor heute, Ph.D. dissertation, Univ. Kiel, Kiel, Germany, 1994.

Seibold, E., and W. H. Berger, *The Sea Floor; An Introduction to Marine Geology*, 2nd ed., Springer–Verlag, New York, 1993.

Seidov, D. G., Numerical modeling of the ocean circulation and paleocirculation, *Mesozoic and Cenozoic Oceans, Geodyn. Ser.*, vol.15, edited by K. J. Hsu, pp. 11–26, AGU, Washington, D. C., 1986.

Seidov, D., An intermediate model for large–scale ocean circulation studies, *Dyn. Atmos. Oceans, 25/1*, 25–55, 1996.

Seidov, D., and R. Prien, A coarse resolution North Atlantic ocean circulation model: An intercomparison study with a paleoceanographic example, *Ann. Geophys.*, *14*, 246–257, 1996.

Seidov, D., M. Sarnthein, K. Stattegger, R. Prien, and M. Weinelt, North Atlantic ocean circulation during the last glacial maximum and subsequent meltwater event: A numerical model, *J. Geophys. Res.*, 101, 16,305–16,332, 1996.

Semtner, A. J., Finite difference formulation of a world ocean model, in *Advanced Physical Oceanographic Modelling*, edited by J. O'Brien, pp. 187–202, D. Reidel, Norwell, Mass. 1986.

Send, U., and J. Marshall, Integral effects of deep convection, *J. Phys. Oceanogr.*, *25*, 855–872, 1995.

Shanks, A. L., and J. D. Trent, Marine snow: Sinking rates and potential role in vertical flux, *Deep Sea Res., Part A, 27*, 137–143, 1980.

Shapiro, R., The use of linear filtering as a parameterization of atmospheric diffusion, *J. Atmos. Sci.*, *28*, 523–531, 1971.

Slowey, N. C., and W. B. Curry, Enhanced ventilation of the North Atlantic subtropical gyre thermocline during the last glaciation, *Nature*, *358*, 665–668, 1992.

Slowey, N. C., and W. B. Curry, Glacial–interglacial differences in circulation and carbon cycling within the upper western North Atlantic, *Paleoceanography*, *10*, 715–732, 1995.

Stocker, T. F., The variable ocean, *Nature*, *367*, 221–222, 1994.

Stommel, H., and A. B. Arons, On the abyssal circulation of the world ocean, II, An idealized model of the circulation pattern and amplitude in the oceanic basins, *Deep Sea Res.*, *6*, 217–233, 1960.

Stull, R. B., Transilient turbulence theory, I, The concept of eddy–mixing across finite distances, *J. Atmos. Sci.*, *41*, 3351–3367, 1984.

Sündermann, J., *North Sea Dynamics*, *Dynamics*, edited by J. Sünderman and W. Lenz , 693 pp., Springer–Verlag, New York, 1983.

Sündermann, J., and R. Klöcker, Sediment transport modeling with applications to the North Sea, in *North Sea Dynamics*, pp. 453–471, Springer–Verlag, New York, 1983.

Syvitski, J. P. M., and T. M. C. Hughes, Delta 2: Delta progadation and basin filling, *Comput. Geosci.*, *18*, 839–897, 1992.

Tetzlaff, D. N., and J. W. Harbaugh, *Simulating Clastic Sedimentation*, Van Nostrand Reinhold, New York, 1989.

Toggweiler, J. R., K. Dixon, and K. Bryan, Simulations of radiocarbon in a coarse–resolution world ocean circulation model, 1, Steady state prebomb distribution, *J. Geophys. Res.*, *94*, 8217–8242, 1989.

Weaver, A. J., and T. M. C. Hughes, Rapid interglacial climate fluctuations driven by North Atlantic ocean circulation, *Nature*, *367*, 447–450, 1994.

Weaver, A. J., and E. S. Sarachik, The role of mixed boundary conditions in numerical models of the ocean's climate, *J. Phys. Oceanogr.*, *21*, 1470–1492, 1991.

Weaver, A. J., J. Marotzke, P. F. Cummins, and E. S. Sarachik, Stability and variability of the thermohaline circulation, *J. . Phys. Oceanogr. , 23*, 39–60, 1993.

Weinelt, M., Veränderungen der Oberflächenzirkulation im Europäischen Nordmeer während der letzten 60.000 Jahre – Hinweise aus stabilen Isotopen, *Ber. 41*, pp. 1–106, Sonderforschungsbereich 313, Univ. Kiel, Kiel, Germany, 1993.

Wold, C. N., Paleobathymetry and sediment accumulation in the northern North Atlantic and southern Greenland–Iceland–Norwegian Sea, Ph.D. thesis, Univ. of Kiel, Kiel, Germany, 1992.

Wright, D., and T. F. Stocker, A zonally averaged ocean model for the thermohaline circulation, I, Model development and flow dynamics, *J. Phys. Oceanogr.*, *21*, 1713–1724, 1991.

Yu, E.-F., R. Francois, and M. P. Bacon, Similar rates of modern and last–glacial ocean thermohaline circulation inferred from radiochemical data, *Nature*, *379*, 689–694, 1996.

Zanke, U., Zusammenhänge zwischen Strömung und Sedimenttransport, Teil 1, Berechnung des Sedimenttransports — allgemeiner Fall —, *Mitt. Franzius Inst. Wasserbau Küsteningeneuerswesen Tech. Univ. Hannover, 47*, 214–345, 1978.

Zhang, S., C. Lin, and R. J. Greatbatch, A thermocline model for ocean–climate studies, *J. Mar. Res.*, *50*, 99–124, 1992.

B. J. Haupt, Sonderforschungsbereich 313, Universität Kiel, Heinrich–Hecht–Platz 10, D–24118 Kiel, Federal Republic of Germany. (e–mail: bernd@sfb313.uni-kiel.de)

D. Seidov, Geologisch–Paläontologisches Intitut, Universität Kiel, Olshausenstraße 40, D–24118 Kiel, Federal Republic of Germany. (e–mail: dan@sfb313.uni–kiel.de)

(Received February 1, 1996; revised September 23, 1996; accepted September 30, 1996.)